# 國 立 交 通 大 學

電子工程學系 電子研究所

碩 士 論 文

# 以第一原理計算分析砷化鎵與磷化銦紅外線雙聲子特徵譜線之研究

# Analysis of two-phonon infrared spectral features of gallium arsenide and indium phosphide by ab initio calculation

研 究 生：林煌翔 Student: Huang-Hsiang Lin

指導教授：顏順通 博士 Advisor: Dr. Shun-Tung Yen

中 華 民 國 一 0 三 年 九 月

# 以第一原理計算分析砷化鎵與磷化銦紅外線雙聲子特徵譜線之研究

# Analysis of two-phonon infrared spectral features of gallium arsenide and indium phosphide by ab initio calculation

研 究 生：林煌翔　　Student: Huang-Hsiang Lin

指導教授：顏順通 博士　　Advisor: Dr. Shun-Tung Yen

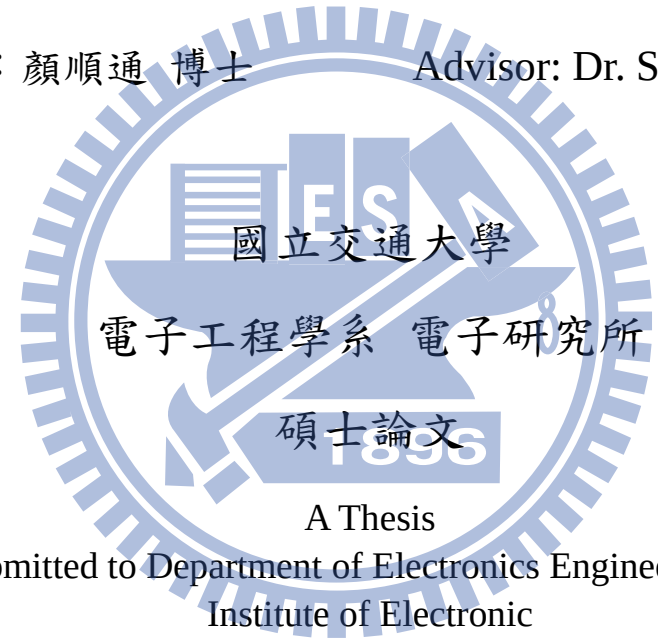

國立交通大學

電子工程學系 電子研究所

碩士論文

A Thesis

Submitted to Department of Electronics Engineering and

Institute of Electronic

College of Electrical and Computer Engineering

National Chiao Tung University

in Partial Fulfillment of the Requirements

for the Degree of

Master of Science

in

Electronic Engineering

September 2014

Hsinchu, Taiwan, Republic of China

中 華 民 國 一 0 三 年 九 月

# 以第一原理計算分析砷化鎵與磷化銦紅外線特徵譜線之研究

學生：林煌翔　　指導教授： 顏順通博士

國立交通大學

電子工程學系 電子研究所 碩士班

## 摘要

我們使用密度泛函微擾理論 (Density functional perturbation theory) 作自洽計算來分析雙聲子過程 (two-phonon process) 對於砷化鎵以及磷化銦在紅外線特頻譜的貢獻，這些特徵譜線可以藉由連結實驗特徵峰值與雙聲子聯合能態密度 (two-phonon joint density of states) 中的范霍夫奇異點 (van Hove singularity) 來完成標記，而我們也分析了在第一布里淵區 (first Brillouin zone) 中的相關臨界點 (critical points)。我們發現砷化鎵以及磷化銦所有的臨界點都只會分布在對稱點 Γ, X, L, W；對稱軸 Σ, Λ, Δ, Q, S; 或是對稱面 ΓKL, ΓXWK, ΓXUL。

# Analysis of two-phonon infrared spectral features of gallium arsenide and indium phosphide by *ab initio* calculations

Student: Huang-Hsiang, Lin Advisor: Shun-Tung, Yen

Department of Electronics Engineering
Institute of Electronics
National Chiao Tung University

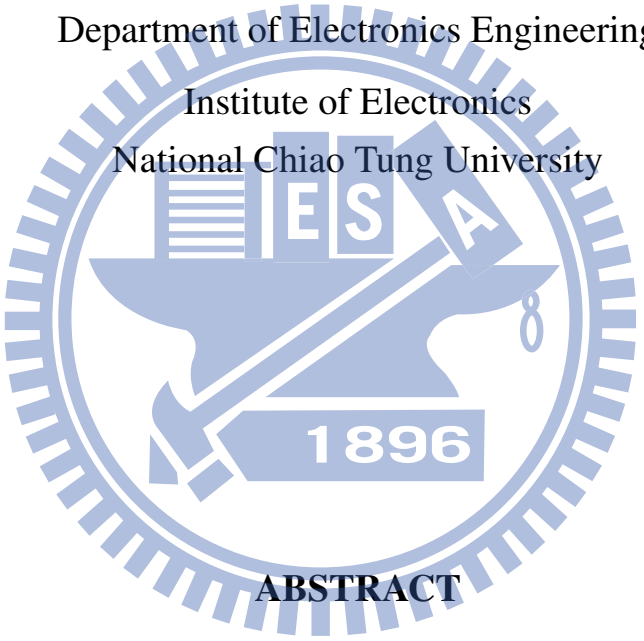

## ABSTRACT

We perform a self-consistent calculation based on the density functional perturbation theory to analyze the infrared spectral features of GaAs and InP contributed by two-phonon processes. Assignment of the features is made by connecting the experimental spectral peaks to the calculated Van Hove singularities of two-phonon joint density of states. The associated critical points in the first Brillouin zone are analyzed. We find that most critical points of GaAs and InP are located at symmetry points of $\Gamma$, X, L and W, symmetry lines of $\Sigma$, $\Lambda$, $\Delta$, Q, and S, or symmetry faces of $\Gamma$KL, $\Gamma$XWK and $\Gamma$XUL.

# Acknowledgments

I would like to thank for my advisor Dr.Shun-Tung Yen for his enthusiastic guidance, immense knowledge and inspiring comments. I learned a lot from his rigorous attitude on scientific research. Also, I would like to thank my friends in the Quantum and Optical Electronics Lab for their help. Finally, I would like show my sincere thankfulness to my parent for their kindness and supporting throughout my life.

# Contents

**Abstract** **i**

**1 Introduction** **1**

**2 Theoretical Approach** **5**

2.1 Density funtional theory . . . . . 6

2.1.1 Kohn-Sham equations . . . . . 6

2.1.2 Local density approximation . . . . . 7

2.2 Density functional perturbation theory . . . . . 7

2.3 Phonons in DFPT . . . . . 9

2.3.1 Interatomic force constant . . . . . 9

2.3.2 Dynamical matrix . . . . . 9

2.4 Two phonon processes . . . . . 10

2.4.1 Two phonon joint dispersion . . . . . 10

2.4.2 Two phonon joint density of states . . . . . 12

2.5 Critical points . . . . . 12

2.5.1 Type $P_0$ critical points . . . . . 12

2.5.2 Type $P_1$ critical points . . . . . 14

2.5.3 Type $P_2$ critical points . . . . . 15

2.5.4 Type $P_3$ critical points . . . . . 16

2.5.5 Type $P$ critical points . . . . . 16
2.6 Technical details . . . . . 17

**3 Results and Discussion** **18**
3.1 Single Phonon Dispersion Relation and Density of States . . . . . 19
3.2 Assignment of 2PDOS's and critical points analysis . . . . . 21
3.2.1 Assignment for GaAs . . . . . 26
3.2.2 Assignment for InP . . . . . 28
3.2.3 Critical Point Analysis . . . . . 31
3.3 Conclusion . . . . . 33

**Appendix** **35**
A.1 Individual two phonon density of states for GaAs . . . . . 36
A.1.1 Sum process . . . . . 36
A.1.2 Difference process . . . . . 38
A.2 Individual two phonon density of states for InP . . . . . 40
A.2.1 Sum process . . . . . 40
A.2.2 Difference process . . . . . 42
A.3 Spectral feature assignment for GaAs . . . . . 44
A.4 Spectral feature assignment for InP . . . . . 50

**Bibliography** **55**

# List of Figures


1.1 The spectrum of electromagnetic wave. Terahertz radiation is ranged from 0.1-10 THz which is between the microwave and infrared. [1] . . . . . 2

1.2 A demonstration of terahertz image through sole and heel.[1] . . . . . 3

1.3 3D imaging of teeth reveals the cavity.[1] . . . . . 3

2.1 Two phonon processes. The sum absorption process involves absorbing a photon, virtually exciting an optically active TO phonon, and eventually decaying into two phonons, while in the difference process the virtually excited TO phonon merges with an existing phonon into a new one. . . . . 11

2.2 Illustration of types of critical points . . . . . 13

3.1 Single-phonon dispersions of (a) GaAs and (b) InP with the density-of-states spectra displayed in the right panels. The curves are obtained by the first-principles calculation. The dots are for neutron scattering data[2, 3]. . . . . 20

3.2 The curve shows an individual two-phonon density of states of GaAs with the branch combination $\nu_1$+$\nu_1$. . . . . 21

3.3 The first Brillouin zone of the face-centered cubic lattice with an irreducible wedge highlighted. . . . . 22

3.4 Type $P_1$ critical point behaviors with different scale cut-off parameter $q_c$ . . . . 23

3.5 The curves demonstrate how a DOS with only type $P_0$ critical point is influenced by the background density of states with type $P_1$ critical point. The blue/dashed curve is the DOS $D_c(\omega)/D_b(\omega)$ with a type $P_0/P_1$ critical point and the red curve represents the superposition of the both DOS. An inflection point has been generated during the superposition. . . . . 24

3.6 The curves demonstrate how a DOS with only type $P_1$ critical point is influenced by the background density of states with type $P_2$ critical point. The blue/dashed curve is the DOS $D_c(\omega)/D_b(\omega)$ with a type $P_1/P_2$ critical point and the red curve represents the superposition of the both DOS. . . . . 25

3.7 The calculated total two-phonon density-of-states spectra of phonon sum processes (in red) and phonon difference processes (in green) for GaAs. Some of the features are indicated with their spectral positions (in $cm^{-1}$), corresponding phonon branch combinations and critical points (in $2\pi$ divided by the lattice constant), symmetry points (or lines, or surfaces) where the critical points are located, and the types of features. The straight red lines in the left panel indicate the spectral positions (in $cm^{-1}$) of absorption features observed by Kotele et al.[4] 27

3.8 The calculated total two-phonon density-of-states spectra of phonon sum processes (in red) and phonon difference processes (in green) for InP. Some of the features are indicated with their spectral positions (in $cm^{-1}$), corresponding phonon branch combinations and critical points (in $2\pi$ divided by the lattice constant), symmetry points (or lines, or surfaces) where the critical points are located, and the types of features. The straight red lines in the left panel indicate the spectral positions (in $cm^{-1}$) of Raman features observed by Bedel et al. [5] 29

3.9 One dimensional phonon dispersion relation of a linear chain in which alternate ions have mass $M_1$ and $M_2$, and only nearest neighbors interact. Two cases of relative order between $M_1$ and $M_2$ have been shown respectively. . . . . 30

3.10 location of critical points projected onto the surface of the irreducible wedge . . 32

A.1 Individual two phonon density of states for GaAs with branches combinations $2\nu_1, \nu_1+\nu_2, \nu_1+\nu_3, \nu_1+\nu_4, \nu_1+\nu_5, \nu_1+\nu_6, 2\nu_2, \nu_2+\nu_3, \nu_2+\nu_4$. . . . . 36
A.2 Individual two phonon density of states for GaAs with branched combinations $\nu_2+\nu_5, \nu_2+\nu_6, 2\nu_3, \nu_3+\nu_4, \nu_3+\nu_5, \nu_3+\nu_6, 2\nu_4, \nu_4+\nu_5, \nu_4+\nu_6, 2\nu_5, \nu_5+\nu_6, 2\nu_6$. . . . . 37
A.3 Individual two phonon density of states for GaAs with branched combinations $\nu_2-\nu_1, \nu_3-\nu_1, \nu_4-\nu_1, \nu_5-\nu_1, \nu_6-\nu_1, \nu_3-\nu_2, \nu_4-\nu_2, \nu_5-\nu_2, \nu_6-\nu_2$. . 38
A.4 Individual two phonon density of states for GaAs with branched combinations $\nu_4-\nu_3, \nu_5-\nu_3, \nu_6-\nu_3, \nu_5-\nu_4, \nu_6-\nu_4, \nu_6-\nu_5$. . . . . 39
A.5 Individual two phonon density of states for InP with branches combinations $2\nu_1, \nu_1+\nu_2, \nu_1+\nu_3, \nu_1+\nu_4, \nu_1+\nu_5, \nu_1+\nu_6, 2\nu_2, \nu_2+\nu_3, \nu_2+\nu_4$. . . . . 40
A.6 Individual two phonon density of states for InP with branched combinations $\nu_2+\nu_5, \nu_2+\nu_6, 2\nu_3, \nu_3+\nu_4, \nu_3+\nu_5, \nu_3+\nu_6, 2\nu_4, \nu_4+\nu_5, \nu_4+\nu_6, 2\nu_5, \nu_5+\nu_6, 2\nu_6$. . . . . 41
A.7 Individual two phonon density of states for InP with branched combinations $\nu_2-\nu_1, \nu_3-\nu_1, \nu_4-\nu_1, \nu_5-\nu_1, \nu_6-\nu_1, \nu_3-\nu_2, \nu_4-\nu_2, \nu_5-\nu_2, \nu_6-\nu_2$. . 42
A.8 Individual two phonon density of states for InP with branched combinations $\nu_4-\nu_3, \nu_5-\nu_3, \nu_6-\nu_3, \nu_5-\nu_4, \nu_6-\nu_4, \nu_6-\nu_5$. . . . . 43

# List of Tables


2.1 Pseudopotential files of the elements Ga, As, In and P. . . . . 17

3.1 The summarized characteristics for the DOS feature type. . . . . 26

3.2 The associated coordinates of symmetry points and symmetry axes. Note that $q_x, q_y, q_z$ are reduced wavevector with unit $2\pi/a$. . . . . 33

A.1 Two phonon spectral feature assignment for GaAs . . . . . 49

A.2 Two phonon spectral feature assignment for InP . . . . . 55

CHAPTER 1

# Introduction

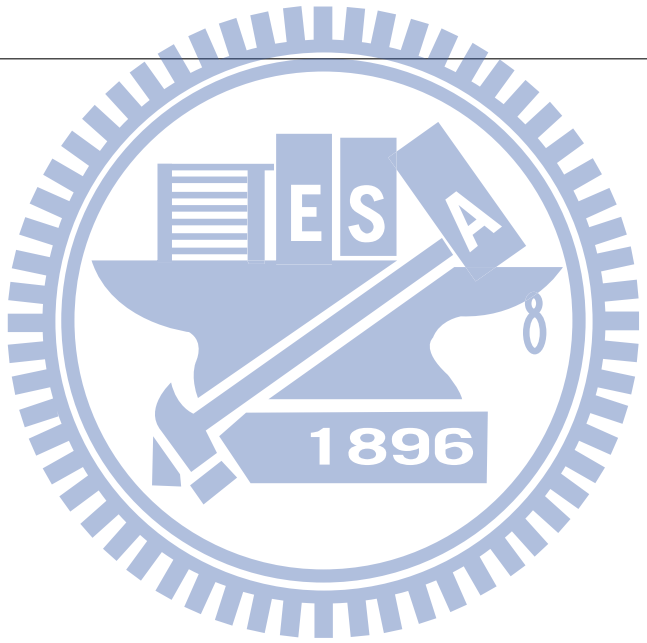

Recently, terahertz/far-infrared radiation has growing applications in many areas such as medical imaging, security, scientific use and communication due to its excellent transmission properties. By definition, it refers to the electromagnetic wave with the frequency range from 0.1-10 THz (see Fig. 1.1) or wavelength from 30 $\mu$m-3mm.

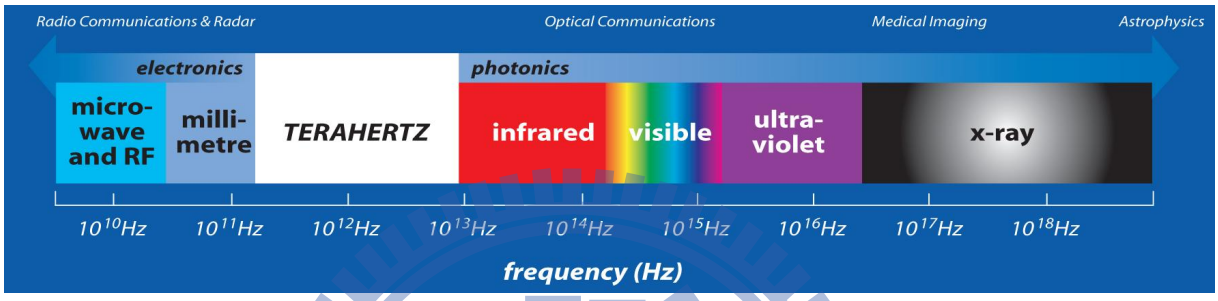


**Figure 1.1:** The spectrum of electromagnetic wave. Terahertz radiation is ranged from 0.1-10 THz which is between the microwave and infrared. [1]

The electromagnetic wave in terahertz regime can penetrate a wide variety of non-metallic materials like clothing, paper, wood, masonry, plastic, ceramic except for water [6]. Therefore, a lot of applications are visible. For example, it can be used in surveillance for uncovering the concealed weapons (see Fig. 1.2). On the other hand, it is a non-ionizing radiation which causes low-damage to human bodies. Hence, it can be applied in medical imaging such as epithelial cancer detection and 3D imaging of teeth (see Fig. 1.3). Moreover, it can be used in high-speed Wi-Fi (40-1200 times faster)[7] due to its large bandwidth. Miscellaneous applications in chemistry and astronomy are also emerging[6].

The optical properties, such as photon absorption/emission, of dielectric crystals in this regime are usually underlain by lattice vibration or, in quantum-mechanical terms, the single/multi-phonon processes.[8] To analyze the problems on phonon, we use the famous *ab initio* methods based on the combination of *density functional theory* (DFT) and *density functional perturbation theory* (DFPT). *Ab initio* methods based on these methods have been common and well


**Figure 1.2:** A demonstration of terahertz image through sole and heel.[1]

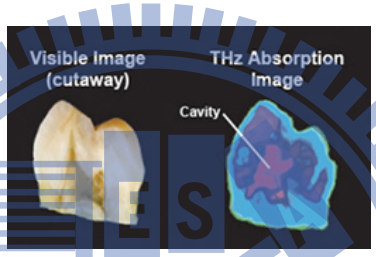


**Figure 1.3:** 3D imaging of teeth reveals the cavity.[1]

established tools for studying vibrational properties of materials. In contrast, early calculations based on empirical modeling approaches, such as the shell model,[9] the bond charge-charge model, [10] and the rigid-ion model [11] have a serious limitation. For instance, the matrix elements in the associated interatomic force constant (electronic part) is usually set as fitting parameters, which are only available with comparing to the experimental dispersion data from neutron scattrering. As a result, they cannot be applied to crystals that are hygroscopic, or difficult to prepare for neutron scattering, such as AlAs. Even for stable materials, exact calculation of phonon dispersion over the whole Brillouin zone is difficult because it requires adjustment of a lot of parameters for fitting to a full-zone set of experimental data of phonon dispersion and usually obtains a much larger deviation in some directions (X-Z-W and W-Q-L). Therefore, the *ab initio* methods become much important in predicting the properties of unfamiliar materials. *Ab initio* method like *frozen-phonon* technique is also able to deal with the problem on phonon. However, it need to construct a supercell commensurate with wavevector $\mathbf{q}$ and will cost much

more computation resources. Hence, DFPT is still by far the most efficient way to solve the problem on phonon.

A lot of related works on phonon have already done recently. For example, Giannozzi et al [12] have first utilized the density functional theory (DFT) together with the linear response method to obtain the phonon dispersion for Si, Ge and many III-V semiconductor materials. Then Deinzer and Strauch[13] have further calculated the absorption spectra for Si and Ge by using DFPT. Moreover, Shirley and Lawler[14] compute the absorption spectra for Si and Ge again and futher assign the features by analyzing the associated critical points for the van Hove singularities. However, a first-principles calculation for the III-V semiconductor materials infrared spectral featrues with critical points analysis is still missing.

In this study, we analyze two-phonon infrared spectral features of III-V semiconductors GaAs and InP. There has been much work on the infrared properties of GaAs and InP, [2, 4, 5, 15–18] but there is still lack of a detailed and convincing analysis of their two-phonon spectral features. We first calculate the phonon dispersions of GaAs and InP using DFPT and then the two-phonon densities of states (2PDOS). The 2PDOS spectra exhibit features strongly related to features in the absorption/emission infrared spectra.[13] The influence of the background DOS to the features are also discussed. As a byproduct, the formation of peak features can also be explained by the superposition of two features. We also perform a critical point analysis to further identify the 2PDOS spectral features. We find an interesting distribution of critical points; all points can only lie on symmetry planes of the reciprocal lattice.

We organize the thesis by first explaining the first-principles method and related theory about density of state in chapter 2. In chapter 3, we discuss the result of our calculation and give a detailed analysis and explanation. The miscellaneous materials such as fully assignment results are put in appendix.

CHAPTER 2

# Theoretical Approach

## 2.1 Density funtional theory

In many-body condense matter physics, the ground state of the electrons in the crystal lattice should be obtained by solving the coupled Schrödinger equation. However, It is technically impossible since the size of the linear system is much too large for the current computation ability. The *density functional theory* (DFT) provides an alternative approach. Instead of solving the eigenstate directly, it puts the emphasis on the charge density $n(\mathbf{r})$ which still preserves a sufficient information of the system.

### 2.1.1 Kohn-Sham equations

In the density functional theory (DFT) framework, the ground state density can be obtained by solving the famous Kohn-Sham equations which read

$$(-\frac{\hbar^2}{2m}\nabla^2 + V_{ext}(\mathbf{r}) + V_H(\mathbf{r}) + \hat{V}_{xc})\psi_i(\mathbf{r}) = \epsilon_i\psi_i(\mathbf{r}),\ i = 1, 2, ..., N \tag{2.1}$$

where $\hbar$ is reduced Planck constant, $m$ is electron mass, $N$ is the number of Kohn-Sham orbitals $\psi_i(\mathbf{r})$, $V_{ext}(\mathbf{r})$ is external potential, $V_H(\mathbf{r})$ denotes Hartree potential and $\hat{V}_{xc}$ is non-local exchange-correlation potential.

$$V_{ext}(\mathbf{r}) = -\sum_I \frac{Z_I e^2}{\mid \mathbf{r} - \mathbf{R}_I \mid} \tag{2.2}$$

$$V_H(\mathbf{r}) = e^2 \int \frac{n(\mathbf{r}')}{\mid \mathbf{r} - \mathbf{r}' \mid} d\mathbf{r}' \tag{2.3}$$

$$\hat{V}_{xc} = \frac{\delta E_{xc}[n(\mathbf{r})]}{\delta n(\mathbf{r})} \tag{2.4}$$

$e$ is the electron charge and $E_{xc}$ denotes the exchange-correlation energy functional and $n(\mathbf{r})$ represents the non-interating system ground state density of electrons. According to the formulation of Kohn-Sham equation, $n(\mathbf{r})$ is identical to the ground state density of interacting many-body system.

### 2.1.2 Local density approximation

In the local density approximation(LDA), the exchange-correlation energy functional is approximated in the form

$$E_{xc}^{LDA}[n(\mathbf{r})] = \int \epsilon_{xc}(n(\mathbf{r}))n(\mathbf{r})d\mathbf{r} \tag{2.5}$$

where $\epsilon_{xc}(n(\mathbf{r}))$ is the many-body exchange-correlation energy density of the interacting homogeneous electron gas. We choose the form of $\epsilon_{xc}(n(\mathbf{r}))$ given by Perdew and Zunger[19] who parametrized the numerical data obtained by Ceperly and Alder [20] with Monte Carlo calculations. And exchange-correlation energy density is written in the sum of exchange contribution $\epsilon_x$ and correlation contribution $\epsilon_c$. For the unpolarized homogeneous electron gas, we have:

$$\epsilon_{xc}(r_s) = \epsilon_x(r_s) + \epsilon_x(r_s) \tag{2.6}$$

$$\epsilon_x(r_s) = -\frac{0.4582}{r_s} \tag{2.7}$$

$$\epsilon_c(r_s) = \begin{cases} -0.1423/(1 + 1.0529\sqrt{r_s} + 0.3334r_s) & r_s \geq 1 \\ -0.0480 + 0.0311\ln r_s - 0.0116r_s + 0.0020r_s \ln r_s & r_s \leq 1 \end{cases} \tag{2.8}$$

In the above expression, engeries are in Hartrees (1 Hartree = 2 Rydbreg); $r_s$ is a dimensionless parameter defined by $(4\pi/3)(r_s a_B)^3 = 1/n$ where $a_B$ denotes the bohr radius. Now we plug Eq.(2.5) into Eq.(2.4), and Eq.(2.4) will become

$$V_{xc}(\mathbf{r}) = \epsilon_{xc}(n(\mathbf{r})) + n(\mathbf{r})\frac{d\epsilon_{xc}(n(\mathbf{r}))}{dn(\mathbf{r})} \tag{2.9}$$

## 2.2 Density functional perturbation theory

The charge density response $\Delta n(\mathbf{r})$ can be obtained self-consistently as a direct generalization of the DFT Kohn-Sham equations. We briefly give the precedure which is usually referred to as the *density functional perturbation theory* (DFPT)[21].

We begin with an initial charge density response and construct the linear correction of Kohn-Sham potential. Then we can solve the equation of first-order perturbation and obtain the first-order variation of Kohn-Sham orbitals. Finally, the updated charge density response can be calculated, which leads to the next step. From the first-order perturbation theory, we have:

$$(H_{KS} - \epsilon_n) |\Delta\psi_n\rangle = -(\Delta V_{KS} - \Delta\epsilon_n) |\psi_n\rangle \tag{2.10}$$

where

$$H_{KS} = -\frac{\hbar^2}{2m}\nabla^2 + V_{ext}(\mathbf{r}) + V_H(\mathbf{r}) + V_{xc}(\mathbf{r}) = -\frac{\hbar^2}{2m}\nabla^2 + V_{KS} \tag{2.11}$$

is the unperturbed Kohn-Sham Hamiltonian,

$$\Delta V_{KS}(\mathbf{r}) = \Delta V_{ext}(\mathbf{r}) + e^2 \int \frac{\Delta n(\mathbf{r}')}{|\mathbf{r} - \mathbf{r}'|} d\mathbf{r}' + \left.\frac{dV_{xc}(n)}{dn}\right|_{n=n(\mathbf{r})} \Delta n(\mathbf{r}) \tag{2.12}$$

is the first-order correction of the Kohn-Sham potential, and $\Delta\epsilon_n = \langle\psi_n| \Delta V_{KS} |\psi_n\rangle$ is the first-order variation of the Kohn-Sham eigenvalue $\epsilon_n$. Note that $\Delta$ means the finite-difference operator which is essentially defined by

$$\Delta^\lambda F = \sum_i \frac{\partial F}{\partial \lambda_i} \Delta\lambda_i \tag{2.13}$$

with the corresponding variable $\lambda_i$.

The charge density can be constructed by the Kohn-Sham orbitals.

$$n(\mathbf{r}) = \sum_{n=1}^{N} |\ \psi_n(\mathbf{r})\ |^2 \tag{2.14}$$

Direct linearizing of Eq.(2.14) gives

$$\Delta n(\mathbf{r}) = 2\mathrm{Re}(\sum_{n=1}^{N} \psi_n^*(\mathbf{r}) \Delta\psi_n(\mathbf{r})) \tag{2.15}$$

Then equations (2.10),(2.12) and (2.15) form a set of self-consistent equations for the perturbed system, which is analogous to the unperturbed Kohn-Sham equations.

## 2.3 Phonons in DFPT

The most important quantity in the beginning of analyzing the properties of phonon is knowing the interatomic force constant or dynamical matrix. We discuss how to obtain these quantity in the following.

### 2.3.1 Interatomic force constant

In the harmonic approximation, the interatomic force constant is by definition

$$C_{i\alpha,j\beta}(\mathbf{R}_I - \mathbf{R}_J) \equiv \frac{\partial^2 E}{\partial u_{s\alpha}(\mathbf{R}_I)\partial u_{t\beta}(\mathbf{R}_J)} \tag{2.16}$$

where the Greek subscripts indicate Cartesian components, s and t represent for the indices of basis atom, $\mathbf{R}_I$ and $\mathbf{R}_I$ mean the coordinates of atomic site I and J, and $E$ is the *Born-Oppenheimer energy surface*, whose Hamiltonian $H_{BO}$ reads

$$\begin{aligned} H_{BO} &= H_e + V_{ion-ion} \\ &= T_e + V_{e-e} + V_{ext} + E_{ion-ion} \\ &= -\frac{\hbar^2}{2m}\sum_i \nabla_i^2 + \frac{e^2}{2}\sum_{i\neq j}\frac{1}{\mid \mathbf{r}_i - \mathbf{r}_j \mid} - \sum_{i,I}\frac{Z_I e^2}{\mid \mathbf{r}_i - \mathbf{R}_I \mid} \\ &\quad + \frac{e^2}{2}\sum_{I\neq J}\frac{Z_I Z_J}{\mid \mathbf{R}_I - \mathbf{R}_J \mid} \end{aligned} \tag{2.17}$$

### 2.3.2 Dynamical matrix

The dynamical matrix is simply given by

$$D_{s\alpha,t\beta}(\mathbf{q}) = \frac{1}{\sqrt{M_s M_t}}\tilde{C}_{s\alpha,t\beta}(\mathbf{q}) \tag{2.18}$$

where $\tilde{C}_{s\alpha,t\beta}(\mathbf{q})$ is the Fourier transform of real space interatomic force constant.

$$\tilde{C}_{s\alpha,t\beta}(\mathbf{q}) = \sum_I C_{s\alpha,t\beta}(\mathbf{R}_I)e^{-i\mathbf{q}\cdot\mathbf{R}_I} \tag{2.19}$$

In the monochromatic perturbation $\mathbf{R}_I[u_s(\mathbf{q})] = \mathbf{R}_l + \tau_s + \mathbf{u_s}(\mathbf{q})e^{i\mathbf{q}\cdot\mathbf{R}_l}$ ($l$ means the $l$-th lattice site, $\tau_s$ is equilibrium position of the s-th atom in the unit cell), we have

$$\begin{aligned}\tilde{C}_{s\alpha,t\beta}(\mathbf{q}) &= \frac{1}{N_c}\frac{\partial^2 E}{\partial u^*_{s\alpha}(\mathbf{q})\partial u_{t\beta}(\mathbf{q})} = \tilde{C}^{el}_{s\alpha,t\beta}(\mathbf{q}) + \tilde{C}^{ion}_{s\alpha,t\beta}(\mathbf{q}) \\ &= \frac{1}{N_c}[\int (\frac{\partial n(\mathbf{r})}{\partial u_{s\alpha}(\mathbf{q})})^* \frac{\partial V_{ext}(\mathbf{r})}{\partial u_{t\beta}(\mathbf{q})} d\mathbf{r} + \int n(\mathbf{r}) \frac{\partial^2 V_{ext}}{\partial u^*_{s\alpha}(\mathbf{q})\partial u_{t\beta}(\mathbf{q})} d\mathbf{r} \\ &\quad + \frac{\partial^2 E_{ion-ion}}{\partial u^*_{s\alpha}(\mathbf{q})\partial u_{t\beta}(\mathbf{q})}] \end{aligned} \tag{2.20}$$

We find that the interatomic force constant in $\mathbf{q}$-space is directly related to the charge density $n(\mathbf{r})$ and charge density response $\partial n(\mathbf{r})/\partial u_\alpha(\mathbf{q})$, which have already been computed by DFT and DFPT calculation. Then we are able to obtained this quantity.

## 2.4 Two phonon processes

The two-phonon processes, including the sum and the difference processes(Fig.2.1), have been known as the underlying mechanism for most features in far-infrared absorption/Raman spectra. The sum absorption process involves absorbing a photon, virtually exciting an optically active TO phonon, and eventually decaying into two phonons, while in the difference process the virtually excited TO phonon merges with an existing phonon into a new one. Energy and momentum conservation are preserved during the process. Since the speed of light is much faster than phonon, the photon momentum can be viewed as zero compared to phonon momentum.

### 2.4.1 Two phonon joint dispersion

The square roots of eigenvalues of the dynamical matrix form the dispersion relation $\omega(\mathbf{q})$. The two-phonon joint dispersion is calculated by:

$$\Omega_{\lambda\pm\lambda'}(\mathbf{q}) = \mid \omega_\lambda(\mathbf{q}) \pm \omega_{\lambda'}(\mathbf{q}) \mid \tag{2.21}$$

where the subscript $\lambda$ is the branch index.

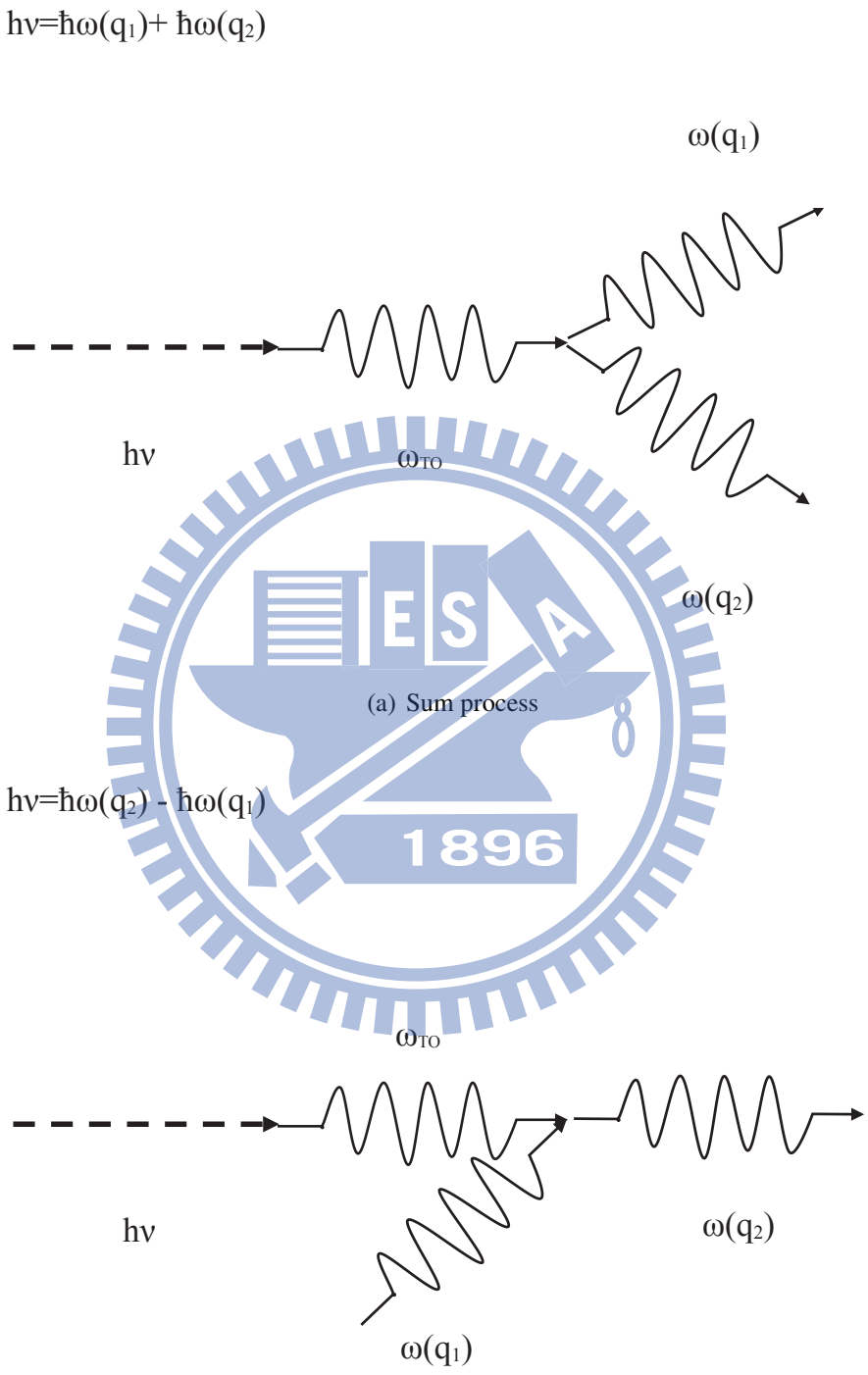


**Figure 2.1:** Two phonon processes. The sum absorption process involves absorbing a photon, virtually exciting an optically active TO phonon, and eventually decaying into two phonons, while in the difference process the virtually excited TO phonon merges with an existing phonon into a new one.

### 2.4.2 Two phonon joint density of states

The 2PDOS can be calculated with the following equaiton:

$$D_{\lambda\pm\lambda'}(\omega) = \frac{V}{(2\pi)^3}\int_{BZ}\delta(\omega - \Omega_{\lambda\pm\lambda'}(\mathbf{q}))d\mathbf{q} \tag{2.22}$$

where $V$ is the volume of crystal and the sign + (-) represents the sum (difference) process and the integration runs over the whole first Brillouin zone.

## 2.5 Critical points

Recall that the formula of density of states can be written as :

$$\frac{V}{(2\pi)^3}\int_{\mathbf{S}(\hbar\omega)}\frac{d\mathbf{S}}{\mid\nabla\hbar\omega(\mathbf{q})\mid} \tag{2.23}$$

where $\mathbf{S}$ is the isoenergy surface with energy $\hbar\omega$. A critical point of a two-phonon joint dispersion $\Omega_{\lambda\pm\lambda'}(\mathbf{q})$ is the one in the reciprocal space at which the gradient of $\Omega_{\lambda\pm\lambda'}(\mathbf{q})$ vanishes. The critical points correspond to van Hove singularities of the 2PDOS spectrum $D_{\lambda\pm\lambda'}(\omega)$.

The dispersion $\omega(\mathbf{k})$ can be expanded about the critical point as

$$\omega(\mathbf{k}) = \omega(\mathbf{k_0}) \pm \frac{1}{2}c_x k_x^2 \pm \frac{1}{2}c_y k_y^2 \pm \frac{1}{2}c_z k_z^2 \tag{2.24}$$

$c_x, c_y, c_z$ are corresponding to the curvature of the phonon dispersion in the x,y and z directions.

The single-phonon DOS spectra have five types of singular features denoted by $P$, $P_0$, $P_1$, $P_2$, $P_3$, respectively. The shapes of all types of critical points are shown in Fig.2.2

### 2.5.1 Type $P_0$ critical points

- $P_0$ denotes a critical points with zero negative sign in the Eq.(2.24), the critical point is a minimum. For type $P_0$ critical points about the frequency $\omega_0$

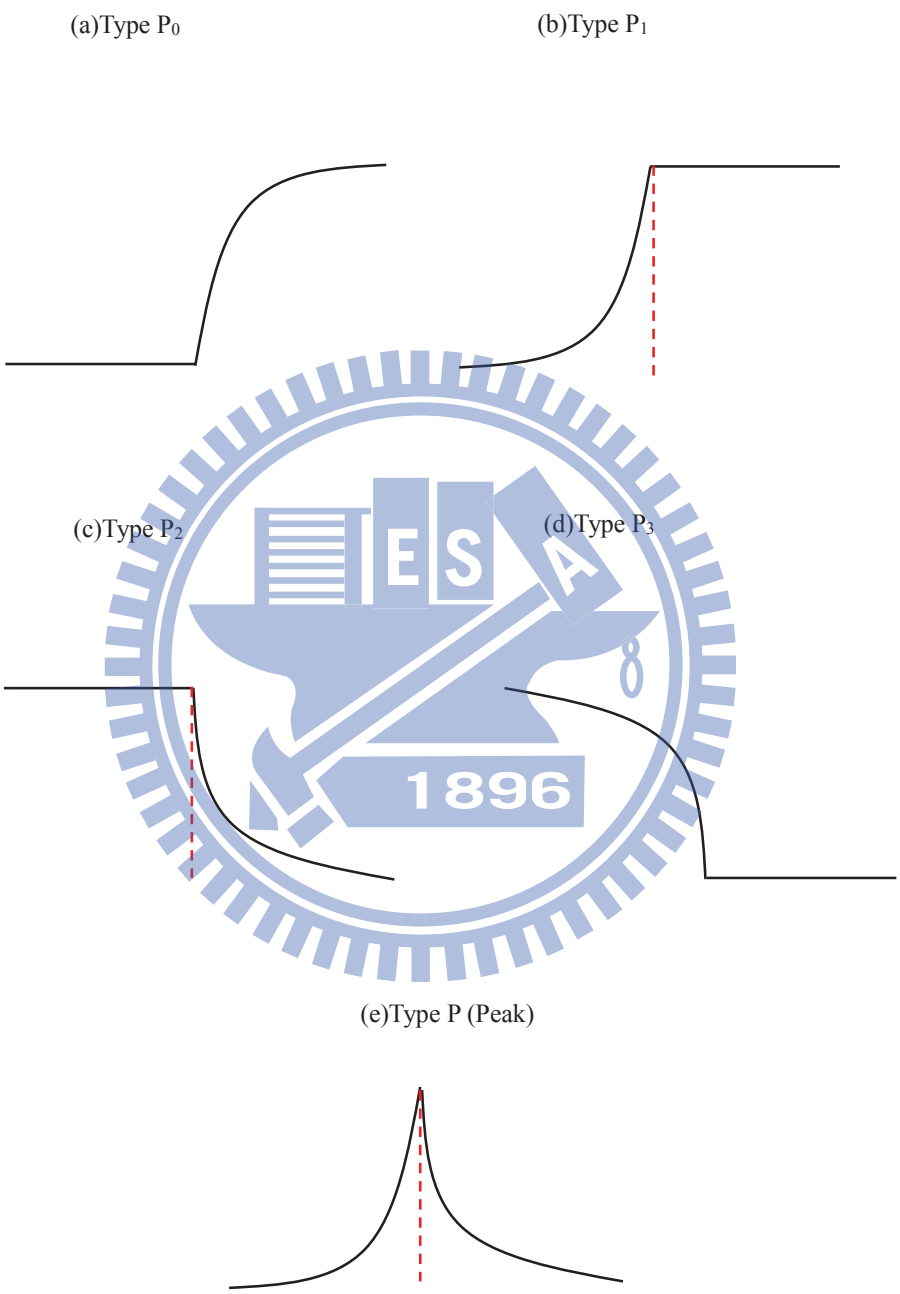


**Figure 2.2:** Illustration of types of critical points

$$
\begin{aligned}
D(\omega) &= \frac{V}{(2\pi)^3}\int \delta(\omega_0 + \frac{1}{2}c_x k_x^2 + \frac{1}{2}c_y k_y^2 + \frac{1}{2}c_z k_z^2 - \omega)d\mathbf{k} \\
&= \frac{V}{(2\pi)^3}\sqrt{\frac{8}{c_x c_y c_z}}\int \delta(\omega_0 + q_x^2 + q_y^2 + q_z^2 - \omega)dq_x dq_y dq_z \\
&= \frac{V}{\pi^2}\sqrt{\frac{2}{c_x c_y c_z}}\int \delta(\omega_0 + q^2 - \omega)q^2 dq \\
&= \frac{V}{\pi^2\sqrt{2c_x c_y c_z}}\int \delta(\omega_0 + u - \omega)\sqrt{u}du \\
&= \begin{cases} \frac{V}{\pi^2\sqrt{2c_x c_y c_z}}\sqrt{\omega - \omega_0} & \omega > \omega_0 \\ 0 & \omega < \omega_0 \end{cases}
\end{aligned} \tag{2.25}
$$

### 2.5.2 Type $P_1$ critical points

- $P_1$ denotes a critical point with a negative sign in the Eq.(2.24), the critical point is a saddle point. For type $P_1$ critical points about the frequency $\omega_1$ :

$$
\begin{aligned}
D(\omega) &= \frac{V}{(2\pi)^3}\int \delta(\omega_1 + \frac{1}{2}c_x k_x^2 + \frac{1}{2}c_y k_y^2 - \frac{1}{2}c_z k_z^2 - \omega)d\mathbf{k} \\
&= \frac{V}{(2\pi)^3}\sqrt{\frac{8}{c_x c_y c_z}}\int \delta(\omega_1 + q_x^2 + q_y^2 - q_z^2 - \omega)dq_x dq_y dq_z \\
&= \frac{V}{\pi^2\sqrt{2c_x c_y c_z}}\int \delta(\omega_1 + q^2 - q_z^2 - \omega)qdqdq_z \\
&= \frac{V}{\pi^2\sqrt{2c_x c_y c_z}}\int \frac{\delta(q_z - \sqrt{\omega_1 + q^2 - \omega}) + \delta(q_z + \sqrt{\omega_1 + q^2 - \omega})}{2\sqrt{\omega_1 + q^2 - \omega}}qdqdq_z \quad , q^2 > \omega - \omega_1 \\
&= \frac{V}{\pi^2\sqrt{2c_x c_y c_z}}\int \frac{qdq}{\sqrt{\omega_1 + q^2 - \omega}} \quad , q^2 > \omega - \omega_1 \\
&= \frac{V}{\pi^2\sqrt{2c_x c_y c_z}}\begin{cases} \int_{\sqrt{\omega-\omega_1}}^{q_c} \frac{qdq}{\sqrt{\omega_1+q^2-\omega}} & \omega > \omega_1 \\ \int_0^{q_c} \frac{qdq}{\sqrt{\omega_1+q^2-\omega}} & \omega < \omega_1 \end{cases}
\end{aligned}
$$

$$
\begin{aligned}
&= \frac{V}{\pi^2\sqrt{2c_xc_yc_z}} \begin{cases} \sqrt{\omega_1 + q_c^2 - \omega} & \omega > \omega_1 \\ \sqrt{\omega_1 + q_c^2 - \omega} - \sqrt{\omega_1 - \omega} & \omega < \omega_1 \end{cases} \\
&= \begin{cases} C_1 & \omega > \omega_1 \\ C_1 - \frac{V}{\pi^2\sqrt{2c_xc_yc_z}}\sqrt{\omega_1 - \omega} & \omega < \omega_1 \end{cases}
\end{aligned} \tag{2.26}
$$

where $q_c$ is a cut-off parameter, and $C_1$ is a smoothly frequency-dependent quantity.

### 2.5.3 Type $P_2$ critical points

- $P_2$ denotes a critical point with two negative signs in the Eq.(2.24), the critical point is a saddle point.

For type $P_2$ critical points about the frequency $\omega_2$

$$
\begin{aligned}
D(\omega) &= \frac{V}{(2\pi)^3}\int \delta(\omega_2 - \frac{1}{2}c_xk_x^2 - \frac{1}{2}c_yk_y^2 + \frac{1}{2}c_zk_z^2 - \omega)d\mathbf{k} \\
&= \frac{V}{(2\pi)^3}\sqrt{\frac{8}{c_xc_yc_z}}\int \delta(\omega_2 - q_x^2 - q_y^2 + q_z^2 - \omega)dq_xdq_ydq_z \\
&= \frac{V}{\pi^2\sqrt{2c_xc_yc_z}}\int \delta(\omega_2 - q^2 + q_z^2 - \omega)qdqdq_z \\
&= \frac{V}{\pi^2\sqrt{2c_xc_yc_z}}\int \frac{\delta(q_z - \sqrt{\omega + q^2 - \omega_2}) + \delta(q_z + \sqrt{\omega + q^2 - \omega_2})}{2\sqrt{\omega + q^2 - \omega_2}}qdqdq_z \quad , q^2 > \omega_2 - \omega \\
&= \frac{V}{\pi^2\sqrt{2c_xc_yc_z}}\int \frac{qdq}{\sqrt{\omega + q^2 - \omega_2}} \quad , q^2 > \omega_2 - \omega \\
&= \frac{V}{\pi^2\sqrt{2c_xc_yc_z}} \begin{cases} \int_0^{q_c} \frac{qdq}{\sqrt{\omega+q^2-\omega_2}} & \omega > \omega_2 \\ \int_{\sqrt{\omega_2-\omega}}^{q_c} \frac{qdq}{\sqrt{\omega+q^2-\omega_2}} & \omega < \omega_2 \end{cases} \\
&= \frac{V}{\pi^2\sqrt{2c_xc_yc_z}} \begin{cases} \sqrt{\omega + q_c^2 - \omega_2} - \sqrt{\omega - \omega_2} & \omega > \omega_2 \\ \sqrt{\omega + q_c^2 - \omega_2} & \omega < \omega_2 \end{cases}
\end{aligned}
$$

$$= \begin{cases} C_2 - \frac{V}{\pi^2\sqrt{2c_xc_yc_z}}\sqrt{\omega-\omega_2} & \omega > \omega_2 \\ C_2 & \omega < \omega_2 \end{cases} \tag{2.27}$$

### 2.5.4 Type $P_3$ critical points

- $P_3$ denotes a critical point with three negative signs in the Eq.(2.24), the critical point is a maximum .

For type $P_3$ critical points about the frequency $\omega_3$

$$\begin{aligned} D(\omega) &= \frac{V}{(2\pi)^3}\int \delta(\omega_3 - \frac{1}{2}c_xk_x^2 - \frac{1}{2}c_yk_y^2 - \frac{1}{2}c_zk_z^2 - \omega)d\mathbf{k} \\ &= \frac{V}{(2\pi)^3}\sqrt{\frac{8}{c_xc_yc_z}}\int \delta(\omega_3 - q_x^2 - q_y^2 - q_z^2 - \omega)dq_xdq_ydq_z \\ &= \frac{V}{\pi^2}\sqrt{\frac{2}{c_xc_yc_z}}\int \delta(\omega_3 - q^2 - \omega)q^2dq \\ &= \frac{V}{\pi^2\sqrt{2c_xc_yc_z}}\int \delta(\omega_3 - u - \omega)\sqrt{u}du \\ &= \begin{cases} 0 & \omega > \omega_3 \\ \frac{V}{\pi^2\sqrt{2c_xc_yc_z}}\sqrt{\omega_3-\omega} & \omega < \omega_0 \end{cases} \end{aligned} \tag{2.28}$$

### 2.5.5 Type $P$ critical points

- $P$ denotes a critical point which can result in ”peak” type of singularity. It can be essentially type $P_1$/$P_2$ critical points. This will be discussed in detail in chapter 3.

| | pseudopotential file |
|---|---|
| Ga | Ga.pz-bhs.UPF |
| As | As.pz-bhs.UPF |
| In | In.pz-hgh.UPF |
| P | P.pz-bhs.UPF |

**Table 2.1:** Pseudopotential files of the elements Ga, As, In and P.

## 2.6 Technical details

Both DFT and DFPT calculation is implemented in the QUANTUM ESPRESSO[22], which is an integrated suite of Open-Source codes for electronic-structure calculations. In the DFT calculations (self-consistent charge density and Kohn-Sham orbitals), we sample the Brillouin zone by the 5×5×5 Monkhorst-Pack special k-point method[23] and we use the norm-conserving type pseudopotential with the LDA exchange-correlation funcitonal proposed by von Barth and Car[24] with 25 Ry cut-off energy. The pseudopotential files can be obtained on the website of QUANTUM ESPRESSO. The files used in our calculation are listed in Table. 2.1. The associated lattice constant we use is 10.49 bohr for GaAs and 11.07 bohr for InP. In the DFPT calculation (especially in the charge density response), we first compute the dynamical matrix on 5×5×5 **q**-point grids. We then perform the Fourier transform from the k-space to the real space and do interpolation. Finally, we compute the dynamical matrix again on the 100×100×100 sampling points. In implementing the integral in Eq.(2.22) to obtain the DOS, the improved tetrahedron method (Blöchl version)[25] is being used. The procedure mentioned above can be achieved by following the guide [26]. However, the two-phonon joint DOS is not implemented. It is mandatory to modify the source code by ourself.

CHAPTER 3

# Results and Discussion

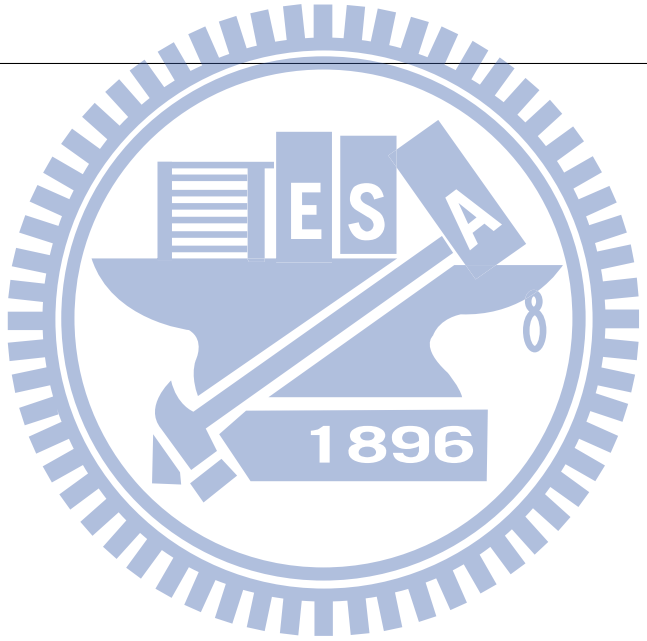

## 3.1 Single Phonon Dispersion Relation and Density of States

The single-phonon dispersion relations of GaAs and InP are shown Fig. 3.1. Since the full dispersion relation is a four dimension manifold, we can only plot the dispersion curve in particular lines. In order to compare to the experimental data given by neutron scattering [2, 3], we choose the six direction Γ-Δ-X, X-Σ-Γ, Γ-Λ-L, L-X, X-Z-W and W-Q-L which are the same to that in their research. The curves are obtained by the first-principles calculation. The dots are for neutron scattering data. The acoustic phonon branches ($\nu_1$,$\nu_2$ and $\nu_3$) for both materials always give an excellent agreement with the experimental data. For optical phonon branches ($\nu_4$,$\nu_5$ and $\nu_6$), calculation results match the experimental data in most directions for GaAs. Even though we use the first-principles calculations, we still have some small discrepancies in X-Z-W and W-Q-L directions. However, it exhibits a great improvement than any other empirical model in this region.[2] For InP, we can only compare the calculation results with experimental data in much fewer directions (Γ-Δ-X, X-Σ-Γ and Γ-Λ-L) due to the limitation of number of the neutron scattering data. As the same case to the GaAs, the curves match well for acoustic mode. For optical mode, the discrepancies are much obvious than that of GaAs. This problem may be due to the choices of the combinations of the proposed the psuedopotentials and exchange-correlation functionals of indium and phosphorus or essentially owing to the reliability of the such limited experimental data. Of course, the same argument can be applied to GaAs to explain the deviation in X-Z-W and W-Q-L directions. We also compute the associated single phonon density of states (DOS) for both materials. The results are shown in the right-hand side of the dispersion curves. As we can see, there is a number of peak corresponding to the flat or less dispersive region in the dispersion relation. This is an expected consequence by the definition of the DOS. From the Eq.(2.23), the vanishing gradient regions give rise to a large amount of contribution to the DOS. On the other hand, We also check our result by comparing to the others' works[21, 27] and we have excellent agreements with them. As a result, we have arrived a steady situation, which is ready for the further analysis of two-phonon joint density of states (2PDOS).

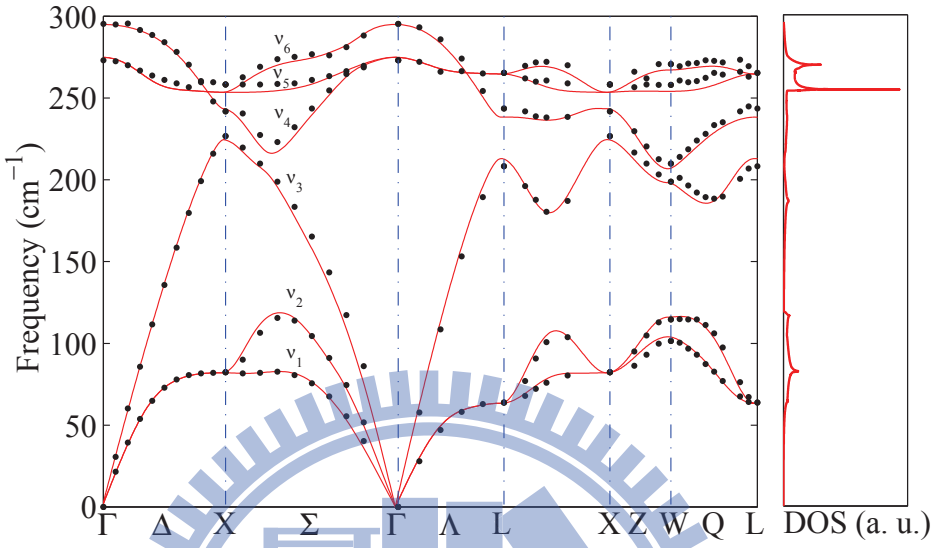


(a) GaAs

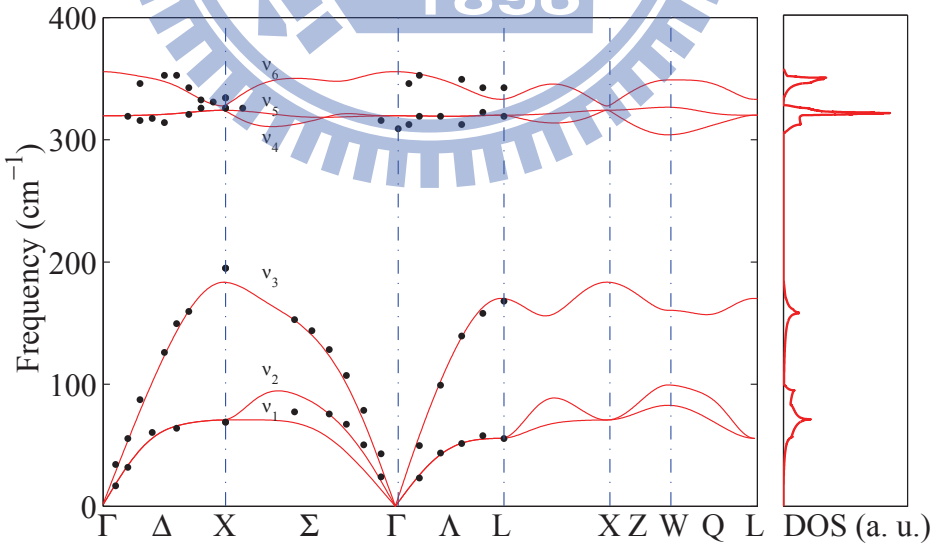


(b) InP

**Figure 3.1:** Single-phonon dispersions of (a) GaAs and (b) InP with the density-of-states spectra displayed in the right panels. The curves are obtained by the first-principles calculation. The dots are for neutron scattering data[2, 3].

## 3.2 Assignment of 2PDOS's and critical points analysis

The assignment scheme is given by the following:

1. Find the van-Hove singularities in the indiviual 2PDOS spectra.

2. Identify the critical point coordinates in two-phonon dispersion relation.

3. Check the whether the critical point frequencies are identical to the singularity positions.

4. Determine the types of the critical points by comparing the nearby behavior to the standard five types of behaviors in Fig. 2.2.

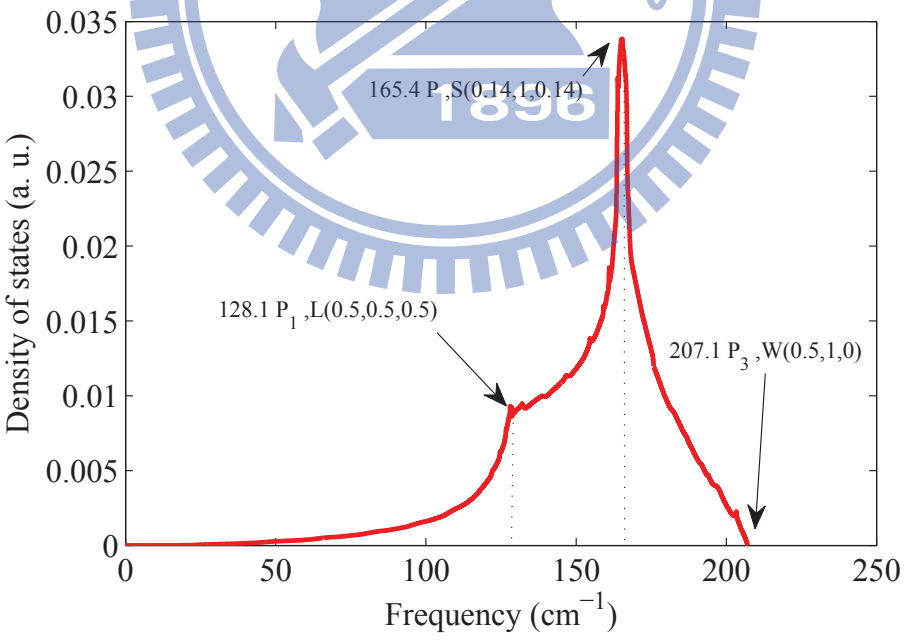


**Figure 3.2:** The curve shows an individual two-phonon density of states of GaAs with the branch combination $\nu_1$+$\nu_1$.

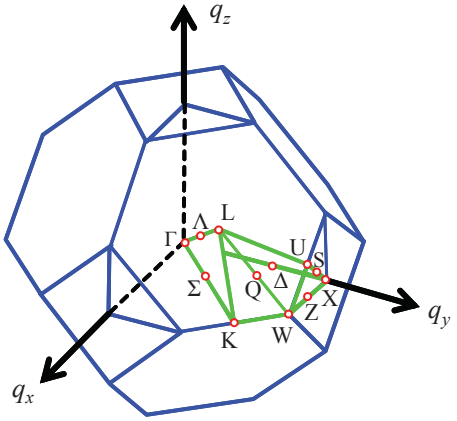


**Figure 3.3:** The first Brillouin zone of the face-centered cubic lattice with an irreducible wedge highlighted.

The example is demonstrated in Fig. 3.2. First, we find out three van-Hove singularities in the curve. The corresponding position of them are 128.1, 165.4 and 207.1 $cm^{-1}$. Secondly, we search the vanishing gradient points in the two-phonon dispersion relation with the branch combination $\nu_1$+$\nu_1$ in the irreducible wedge (the truncated octahedron in Fig. 3.3). We find that the critical points are located at L(0.5,0.5,0.5), S(0.14,1,0.14) and W(0.5,1,0). In the third step, we check the corresponding frequencies of these critical points whether they are exactly or approximately equal to the singularity positions in step 1. If the deviation is acceptable (within 5% tolerance), then we will assign this feature. In this case, the corresponding frequencies at L(0.5,0.5,0.5), S(0.14,1,0.14) and W(0.5,1,0) are 126.78, 163.35 and 208.00 $cm^{-1}$ respectively. With this observation, we can easily attribute the van-Hove singularities at 128.1, 165.4 and 207.1 $cm^{-1}$ to the corresponding critical points L(0.5,0.5,0.5), S(0.14,1,0.14) and W(0.5,1,0) respectively. In the final step, we have to determine the types of the critical points by comparing the nearby behaviors to the standard type $P_0$ (minimum), $P_1$ (saddle point), $P_2$ (saddle point), $P_3$ (maximum) and $P$ (peak) critical points (see Fig. 2.2). For instance, the behavior of critical point at 128.1 $cm^{-1}$ manifests an similar shape to that in Fig. 2.2(b), which is concave upward on the left-hand side (behavior on the right-hand side is less important and this point

(a) large $q_c$ (b) medium $q_c$

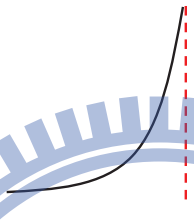

(c) small $q_c$

**Figure 3.4:** Type $P_1$ critical point behaviors with different scale cut-off parameter $q_c$

will be discussed later). The same procedure can be applied to the other two van-Hove singularities. For critical point at 165.4 cm$^{-1}$, it shows an prominently sharp behavior similiar to that in Fig. 2.2(e), which is a nondifferentiably local maximum. For critical point at 207.1 cm$^{-1}$, it exhibits an similar behavior to that in Fig. 2.2(d), which is vanishing on the right-hand side and increasing (concave downward) on the left-hand side.

For a type $P_1$ critical point, the behavior on the right-hand side is less important. This is because that the smoothly frequency-dependent quantity $C_1$ in Eq.(2.26) contains the cut-off parameter $q_c$. $C_1$ behaves like a constant, when $q_c$ is large enough which means the nearby dispersion relation:

$$\omega(\mathbf{k}) = \omega(\mathbf{k_0}) + \frac{1}{2}c_x k_x^2 + \frac{1}{2}c_y k_y^2 - \frac{1}{2}c_z k_z^2 \tag{3.1}$$

holds the validity in the much wider region. In contrast, $C_1$ becomes vanishing when $q_c$ is small which means the dispersion relation in the vicinity holds its validity much narrower domain. Based on this fact, the right-hand side behavior of a type $P_1$ critical point is dependent on the

*region of validity* of Eq.(3.1). However, the the left-hand side behavior is always concave upward regardless of the region of validity. Therefore, we can conclude that the left-hand side behavior is always concave upward in any situation. This argument can apply to the type $P_2$ critical point as well. We can claim that the behavior on the left-hand side is less important. On the contrary, we face no difficulty upon assigning the type $P_0$, $P_3$ and $P$ critical points since they have well-defined behaviors on the both side.

There is one relevant effect for us to consider which is the influence of the background density of states. The background density of states will smoothly influence the behavior of critical points. The reason for the cause of background density of state can be simply due to the other critical points or essentially by the dispersion behavior beyond the standard quadratic form in Eq.(2.24). The latter one is much difficult to discuss due to the arbitrariness of the function form of dispersion. On the contrary, the former one can be illustrated in the Fig. 3.5.

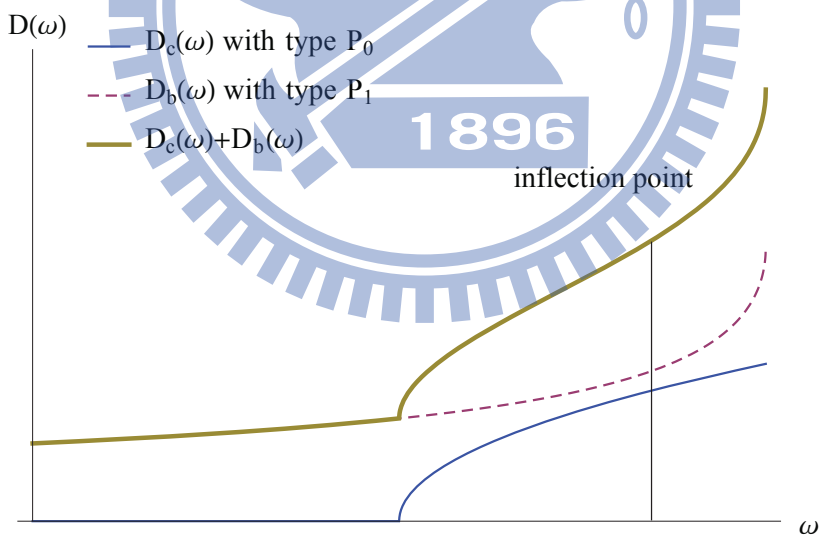


**Figure 3.5:** The curves demonstrate how a DOS with only type $P_0$ critical point is influenced by the background density of states with type $P_1$ critical point. The blue/dashed curve is the DOS $D_c(\omega)$/$D_b(\omega)$ with a type $P_0$/$P_1$ critical point and the red curve represents the superposition of the both DOS. An inflection point has been generated during the superposition.

As we can see, behavior of superposition of the background DOS and the small region DOS with the type $P_0$ critical point has slightly different to the original DOS but it will not affect too much to our assigning criterion. Note that an inflection point may be potentially generated due to the competition of the concavity of the both DOS. If the background concavity can flip the direction of the original concavity, then an inflection point will be generated and will not affect the DOS too much.

Let's see the next example. A DOS $D_c(\omega)$ with type $P_1$ critical point on the left-hand side is superimposed by another DOS $D_b$ with type $P_2$ critical point on the right-hand side. The process is demonstrated in the Fig. 3.6. We can find that there are two features on the total DOS $D_c(\omega) + D_b$ and observe that the peak at the feature 1 is essentially caused by the type $P_1$ critical point. Based on this concept, the peak behavior can be explained. Notice that the total DOS can not be ploted in full region since the individual DOS's are only simultaneously well-defined in some region.

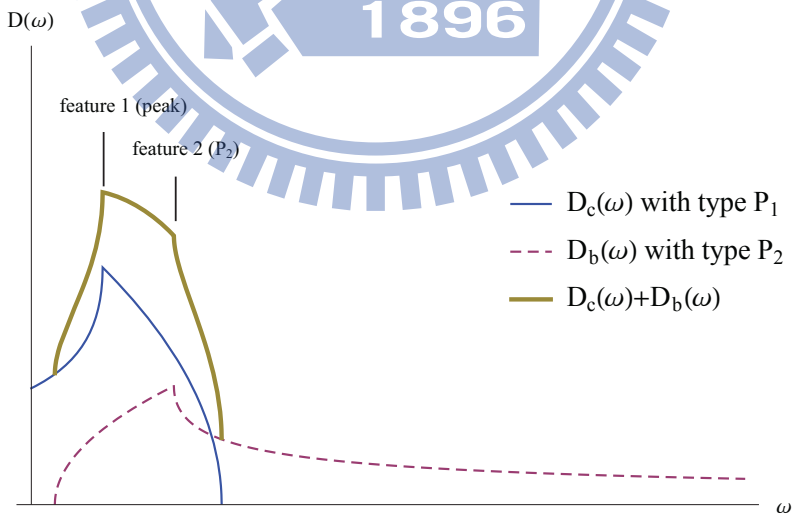


**Figure 3.6:** The curves demonstrate how a DOS with only type $P_1$ critical point is influenced by the background density of states with type $P_2$ critical point. The blue/dashed curve is the DOS $D_c(\omega)/D_b(\omega)$ with a type $P_1/P_2$ critical point and the red curve represents the superposition of the both DOS.

| | Dispersion behavior | Left-hand side DOS | Right-hand side DOS |
|---|---|---|---|
| Type $P_0$ | minimum | vanishing/varying | concave downward |
| Type $P_1$ | saddle point | concave upward | varying |
| Type $P_2$ | saddle point | varying | concave upward |
| Type $P_3$ | minimum | concave downward | vanishing/varying |
| Type $P$ (peak) | saddle point | varying | varying |

**Table 3.1:** The summarized characteristics for the DOS feature type.

Now we can fairly say that the feature shape of a critical point would be influenced slightly but still preserves part of the original behaviors. We summarize the criterion of type identification in the Table. 3.1. Note that even though the feature shape of a peak are varying on the both side, a nondifferentiably local maximum is still a clear characteristic.

Now we are able to specify the features for all of the individual 2PDOS for GaAs and InP. After a very tedious work, we find out 124 features for GaAs and 117 features for InP. The assignment is all listed in the appendix. On the other hand, the relatively prominent features of the total 2PDOS is also identified and shown in Fig. 3.7 and Fig. 3.8. As we can see, there are two types of curves. One (in red) corresponds to the sum process, and the other (in green) to the difference process. There are plenty of experimental peaks in the spectra which are connected to the Van Hove singularities.

### 3.2.1 Assignment for GaAs

For GaAs, we can see a plenty of solid red straight lines on the left-hand side in Fig. 3.7 which are the experimental feature positions obtaining by Kotele et al [4] via infrared absorption measurement. The data are ranging from 108 $cm^{-1}$ to 590 $cm^{-1}$ and there is no observation of peak between 235 $cm^{-1}$ to 310 $cm^{-1}$. This is due to that the photons have a strong resonance with

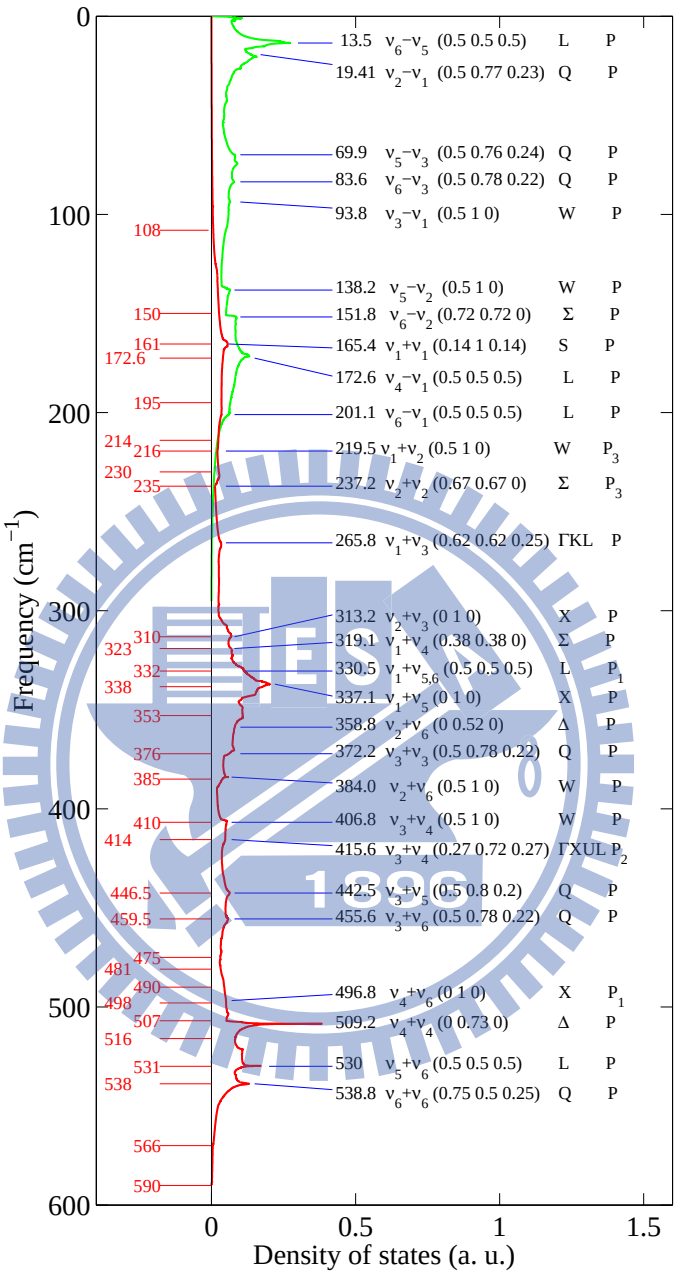


**Figure 3.7:** The calculated total two-phonon density-of-states spectra of phonon sum processes (in red) and phonon difference processes (in green) for GaAs. Some of the features are indicated with their spectral positions (in cm$^{-1}$), corresponding phonon branch combinations and critical points (in $2\pi$ divided by the lattice constant), symmetry points (or lines, or surfaces) where the critical points are located, and the types of features. The straight red lines in the left panel indicate the spectral positions (in cm$^{-1}$) of absorption features observed by Kotele et al.[4]

the TO phonons in this region which is so-called *reststrahlen band*. Therefore, the light cannot penetrate through the material and cause the transmittance become approximately zero. On the other hand, the material will also reflect the light strongly and give a roughly unity reflectance. Since the absorption coefficient depends on the transmittance, it will be very sensitive to the background noise and cause a large deviation and unreliable data. That's the reason why they report empty peak in this region. For the other observed features, we can see that many of the experimental data have been assigned. For example, a feature assigned at 150 $cm^{-1}$ in the left-hand side of the Fig. 3.7 and the phonon peak position carried out by our calculation is 151.8 $cm^{-1}$ which somewhat indicates a successfulness of our analysis. Besides, the associated branch combination and critical point are $\nu_6 - \nu_2$ and (0.72,0.72,0) (on the $\Sigma$ axis). Now, we can clearly explain how the peak here is formed. In the beginning, a incoming photon carried with the frequency (energy) about 150 $cm^{-1}$ scatters with the GaAs lattice, and transforming into an virtually excited TO phonon. Then the intermediate phonon scatters another existed acoustic phonon mode $\nu_2$ with wavevector or momentum at (0.72,0.72,0) (in $2\pi/a$ $cm^{-1}$) and they combine together become an new optical phonon mode $\nu_2$ with the same wavevector or momentum at (0.72,0.72,0) due to the momentum conservation (the photon momentum is roughly zero or negligible compared to that of phonon). There is one point for us to know that the low frequency data below 108 $cm^{-1}$ are missing due to the experimental limit but we can still give a clear result which is dominated by difference process. For the region inside the reststrahlen band, we have also observed some features. As a result, the features in low frequency region or inside reststrahlen band can be predicted and may be observed by the improvement of the experiment.

### 3.2.2 Assignment for InP

As for InP, most of the mentioned descriptions can read from the Fig. 3.8 and the procedure is all most the same. As this time, the experimental data is obtained from Bedel et al [5] via Ra-

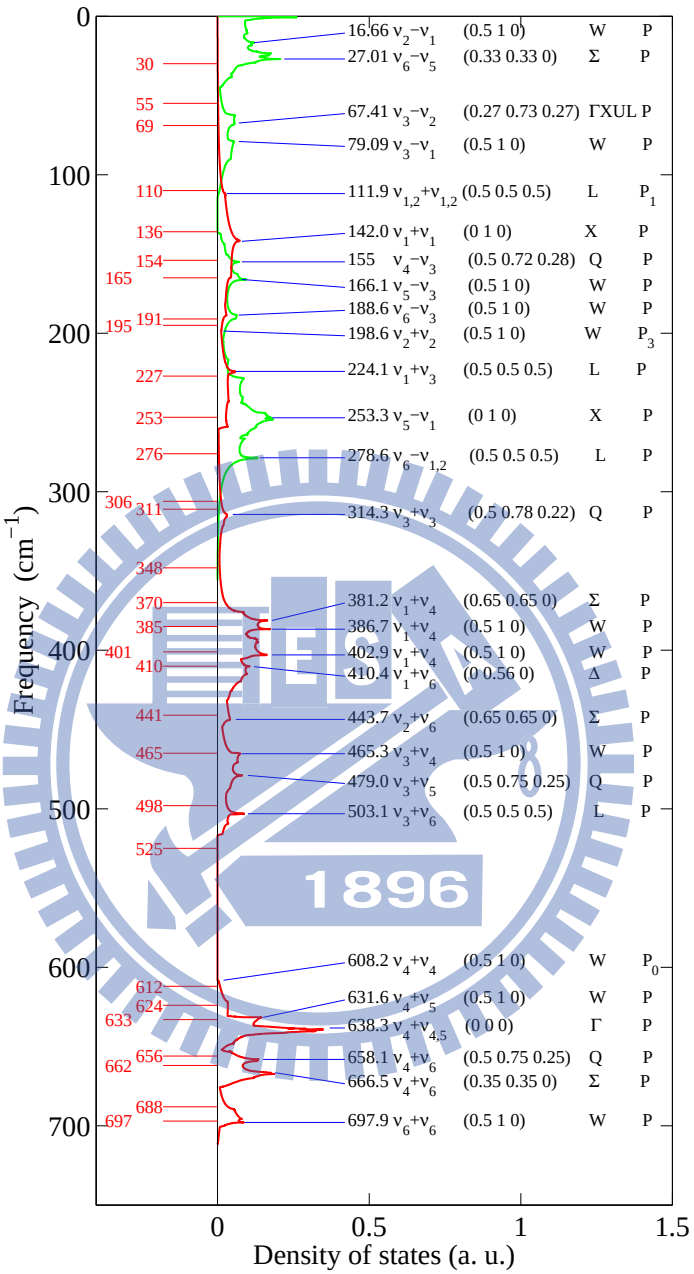


**Figure 3.8:** The calculated total two-phonon density-of-states spectra of phonon sum processes (in red) and phonon difference processes (in green) for InP. Some of the features are indicated with their spectral positions (in cm$^{-1}$), corresponding phonon branch combinations and critical points (in $2\pi$ divided by the lattice constant), symmetry points (or lines, or surfaces) where the critical points are located, and the types of features. The straight red lines in the left panel indicate the spectral positions (in cm$^{-1}$) of Raman features observed by Bedel et al. [5]

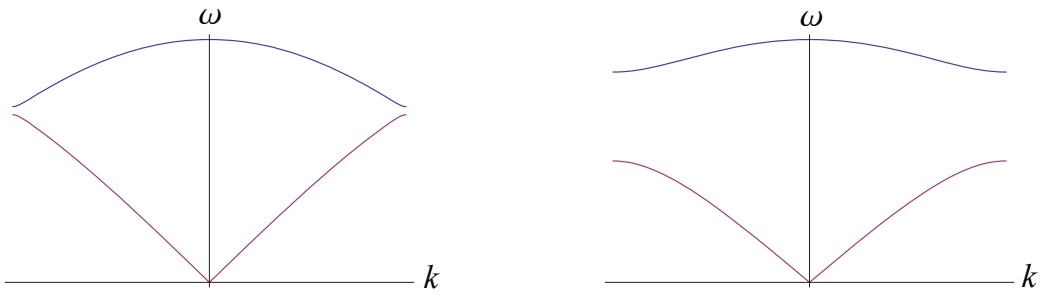


(a) $M_1 \approx M_2$ (b) $M_1 \gg M_2$

**Figure 3.9:** One dimensional phonon dispersion relation of a linear chain in which alternate ions have mass $M_1$ and $M_2$, and only nearest neighbors interact. Two cases of relative order between $M_1$ and $M_2$ have been shown respectively.

man spectroscopy instead of infrared absorption. Since the wavelength of Raman experiment is around visible light which is completely different order compared to infrared and the measurement is based on the scattering of light instead of absorption, it will not face with the problem of reststrahlen effect. The data are ranging from 30 $cm^{-1}$ to 697 $cm^{-1}$. It is noteworthy that they still observed a gap between 525 and 612 $cm^{-1}$ and we also obtain a very similiar result. This is a called the fingerprint of semiconductor. The basic reason of this phenomenon is owning to the large mass difference (e.g. $M_{In} = 114.818\ amu \gg M_P = 30.947\ amu$). Such semiconductors have much less dispersive optical phonon branches and a wider gap than other semiconductors, such as GaAs ($M_{Ga} = 69.72\ amu \approx M_{As} = 74.92\ amu$). This can easily be explained in one dimensional case. Consider a linear chain in which alternate ions have mass $M_1$ and $M_2$, and only nearest neighbors interact with string constant $K$. One can use the classical model to show that the dispersion relation for the normal modes is :

$$\omega(k) = \sqrt{\frac{K}{M_1 M_2}(M_1 + M_2 \pm \sqrt{M_1^2 + M_2^2 + 2M_1 M_2 \cos ka})} \tag{3.2}$$

where $a$ represents the lattice constant. Two extreme cases for relative order between $M_1$ and $M_2$ have been shown in Fig. 3.9. The fact that the gap is much wider than each of the optical phonon branches, as shown in Fig 3.1, causes the fingerprints in the two-phonon DOS spectrum

of InP. Be more specific, the fingerprint will appear when the condition $\Omega_{\nu_4+\nu_4}(\mathbf{k}) > \Omega_{\nu_3+\nu_6}(\mathbf{k})$ holds for every k-point in the first Brillouin zone, which means we cannot form a possible linear combination of the branches and give a contribution to the 2PDOS in the fingerprint region. In appendix, this condition is also held.

### 3.2.3 Critical Point Analysis

The cubic symmetry of the crystals allows us to consider only the critical points in the irredicible wedge of the first Brillouin zone as shown in Fig. 3.3. The wedge is one of 48 equivalent parts of the first Brillouin zone and enclosed by five symmetry planes with respective to which reflection leaves the reciprocal lattice invariant.

Specifically, we choose the wedge with the following condition:

$$q_z \geq 0, \quad q_x + q_y + q_z \leq 3/2, \quad q_y \leq 1, \quad q_x \leq q_y, \quad q_z \leq q_x$$

The associated coordinates of symmetry points and symmetry axes are listed in Table 3.2. Interestingly, a very important phenomenon has been observed: *All critical points are only located at symmetry points, on symmetry axes or on symmetry faces*. No critical point inside the irreducible wedge of the first Brillouin zone(Fig. 3.3) is being found, which means the extrema and saddle points will *only* appear in these high symmetry domain and this is a reasonable discovery. Although the phenomenon may be elegantly explained by the space group, however, it is beyond our discussion.

Since all the critical points are located on the surface of the irreducible wedge of fcc first Brillouin zone, it is straightforward to make a scatter plot of the critical points which is shown in Fig.3.10. As we can see, critical points manifest an aggregation behavior, which means a critical point would be usually accompanied by other critical points in the vicinity. This is due to that the vanishing gradient criterion is replaced by a small tolerance value in practical, which depends on the critical points locations. Some critical points simply need small tolerance and

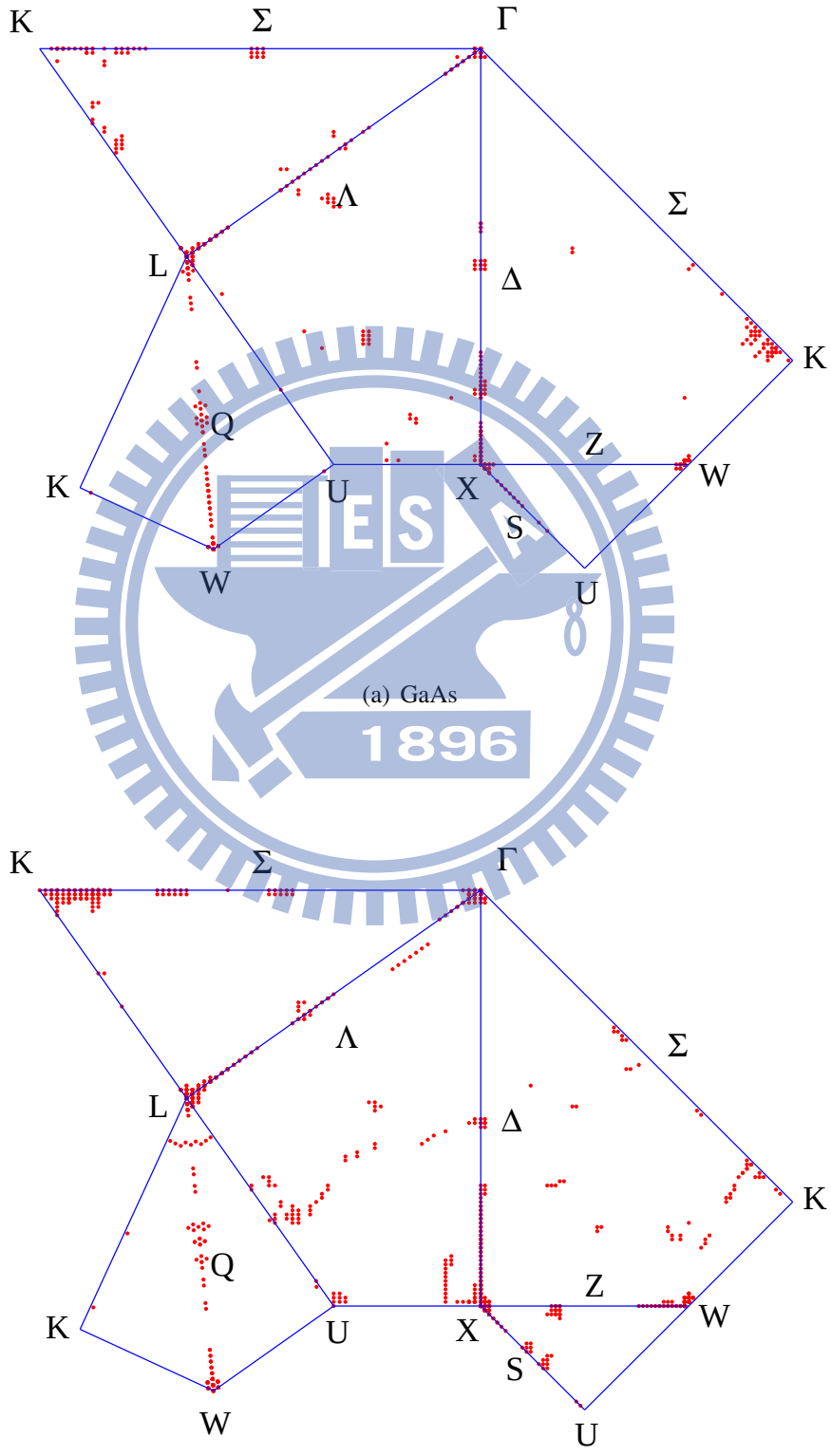


(a) GaAs

(b) InP

**Figure 3.10:** location of critical points projected onto the surface of the irreducible wedge

| symmetry points | | symmetry axes | | | symmetry faces |
|---|---|---|---|---|---|
| Γ | (0,0,0) | Z (X-W) | ($\xi$,1,0) | ΓXUL | $q_x = q_z$ |
| X | (0,1,0) | Δ (Γ-X) | (0,$\xi$,0) | ΓXWK | $q_z = 0$ |
| K | (0.75,0.75,0) | Σ (Γ-K) | ($\xi$,$\xi$,0) | ΓKL | $q_x = q_y$ |
| L | (0.5,0.5,0.5) | Λ (Γ-L) | ($\xi$,$\xi$,$\xi$) | LUWK | $q_x + q_y + q_z = 3/2$ |
| W | (0.5,1,0) | Q (L-W) | (0.5,1-$\xi$,$\xi$) | XWU | $q_y = 1$ |
| U | (0.25,1,0.25) | S (U-X) | ($\xi$,1,$\xi$) | | |

**Table 3.2:** The associated coordinates of symmetry points and symmetry axes. Note that $q_x, q_y, q_z$ are reduced wavevector with unit $2\pi/a$.

the other way around. This implies the curvature depends on the location of the critical point. Therefore, it will cause the numbers of points in aggregation are much more in somewhere. This problem can be simply resolved by dynamically adjusting the tolerance value to limit the number of points in aggregation with a acceptable threshold value (in our analysis the value is 10).

The distribution of the critical points are also interesting. In Fig.3.10(a), the critical point responsible for the features of GaAs are mainly located around symmetry point L,W,X and Γ. Some of them lie on Σ, Δ, Q, Λ and S axis. The others reside on symmetry faces ΓKL, ΓXWK and ΓXUL. As for InP, the distribution is roughly similiar to that of GaAs since they are both zincblende structure and with similar profile of dispersion manifold.

## 3.3 Conclusion

We have performed a convincing analysis of far-infrared features resulting from two-phonon processes for GaAs and InP. The phonon dispersions have been calculated exactly by DFPT. The resulting 2PDOS spectra can successfully explained many observed features from either

infrared absorption or Raman scattering measurement, and further give a prediction beyond the limit of experiment. We have also identified the features by assigning them the corresponding two-branch combinations, the critical points, and the types of critical points. The analysis indicates that phonons of wave vectors around symmetry points and along symmetry lines are collectively responsible for strong infrared features in two-phonon processes.

# Appendix

# A.1 Individual two phonon density of states for GaAs

## A.1.1 Sum process

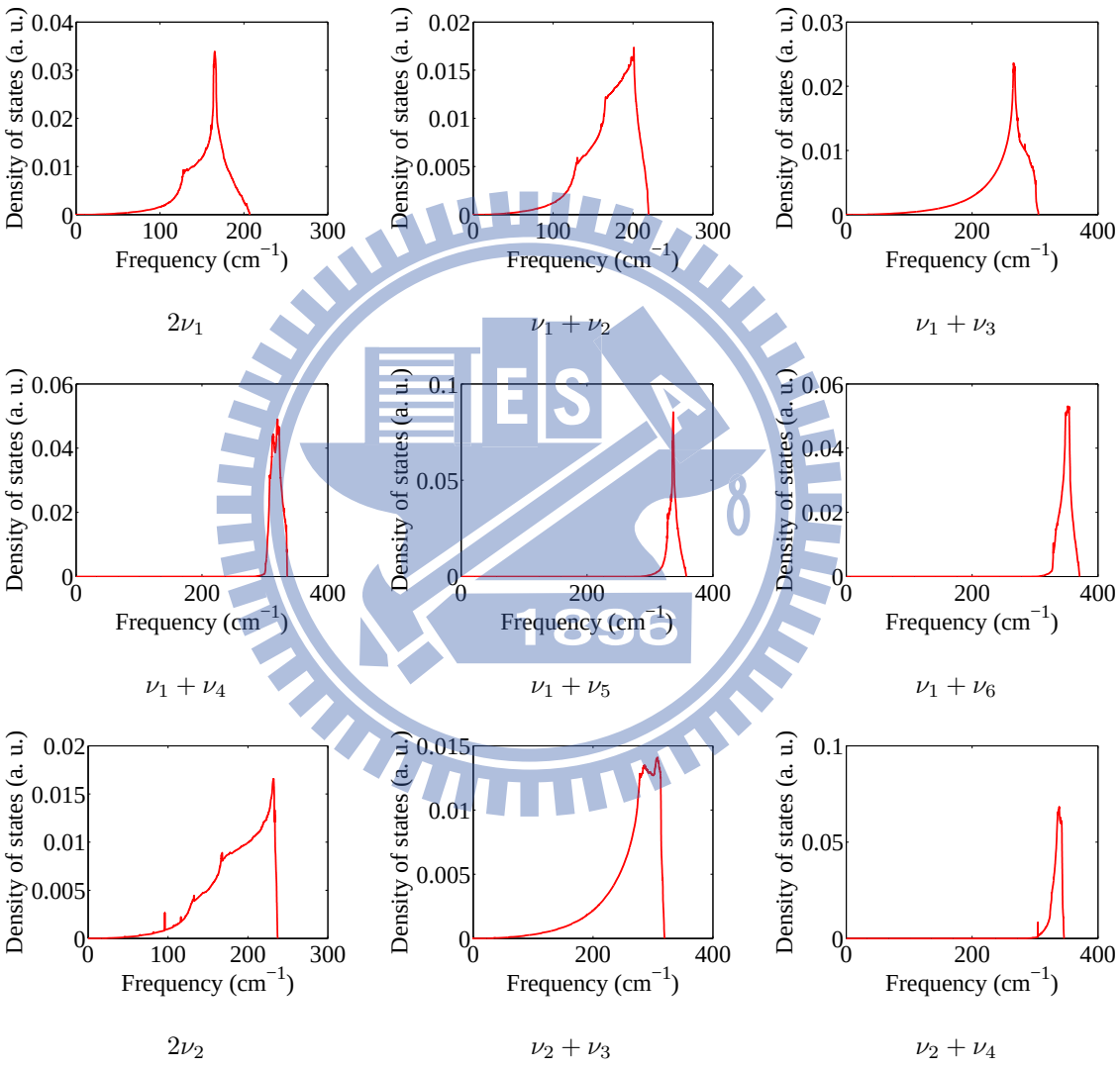


**Figure A.1:** Individual two phonon density of states for GaAs with branches combinations $2\nu_1$, $\nu_1 + \nu_2$, $\nu_1 + \nu_3$, $\nu_1 + \nu_4$, $\nu_1 + \nu_5$, $\nu_1 + \nu_6$, $2\nu_2$, $\nu_2 + \nu_3$, $\nu_2 + \nu_4$.

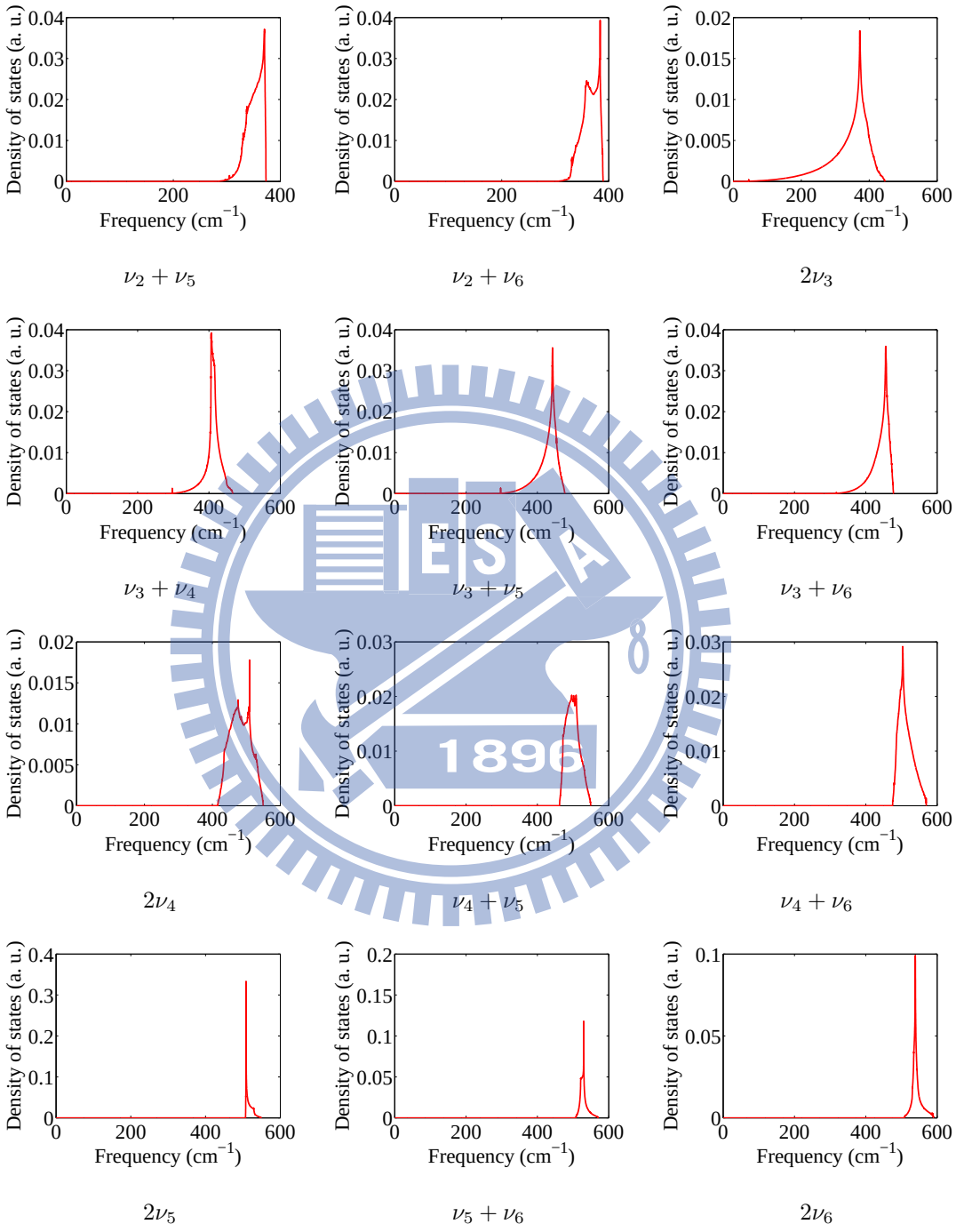


**Figure A.2:** Individual two phonon density of states for GaAs with branched combinations $\nu_2 + \nu_5$, $\nu_2 + \nu_6$, $2\nu_3$, $\nu_3 + \nu_4$, $\nu_3 + \nu_5$, $\nu_3 + \nu_6$, $2\nu_4$, $\nu_4 + \nu_5$, $\nu_4 + \nu_6$, $2\nu_5$, $\nu_5 + \nu_6$, $2\nu_6$.

### A.1.2 Difference process

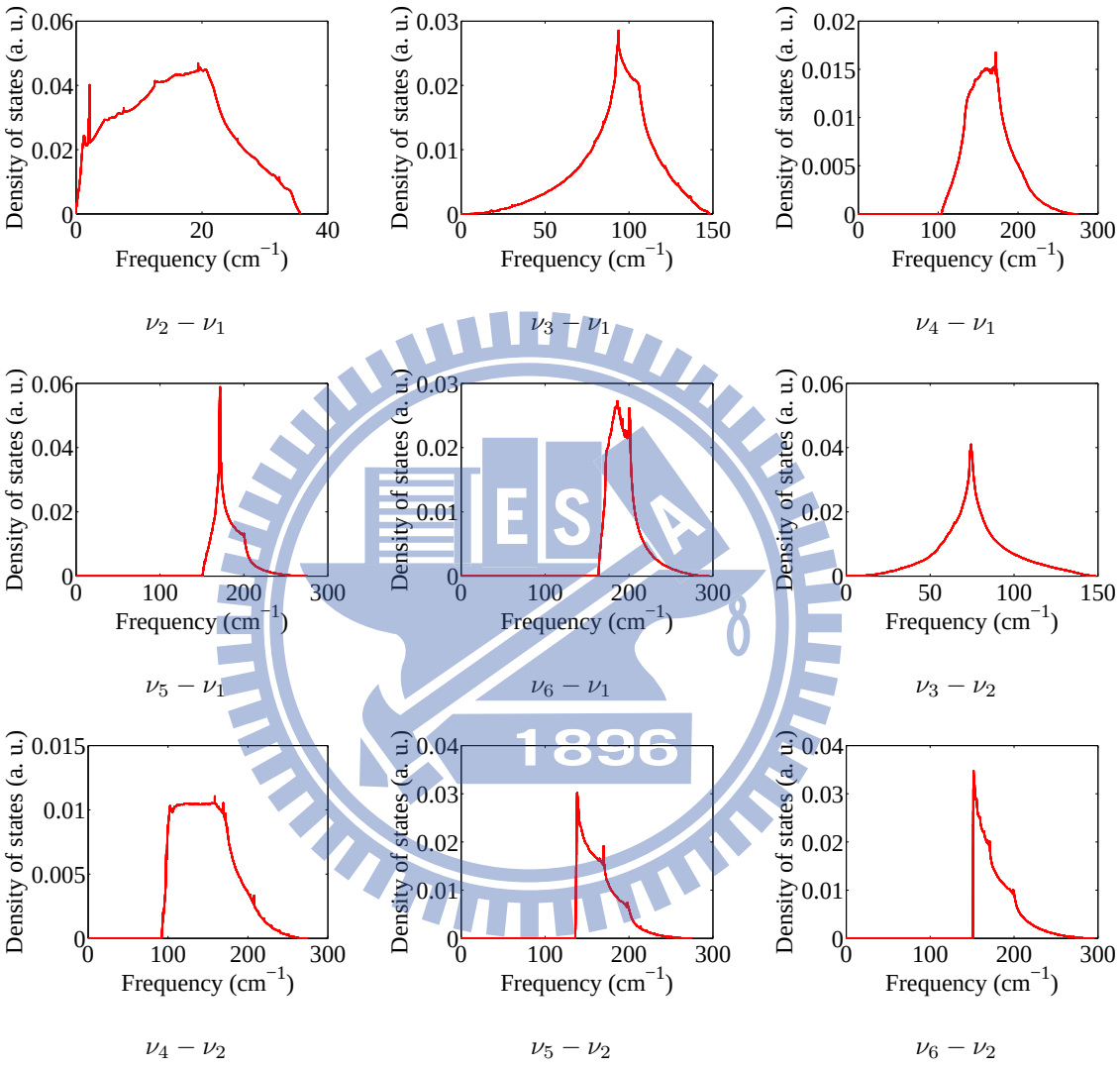


**Figure A.3:** Individual two phonon density of states for GaAs with branched combinations $\nu_2 - \nu_1$, $\nu_3 - \nu_1$, $\nu_4 - \nu_1$, $\nu_5 - \nu_1$, $\nu_6 - \nu_1$, $\nu_3 - \nu_2$, $\nu_4 - \nu_2$, $\nu_5 - \nu_2$, $\nu_6 - \nu_2$.

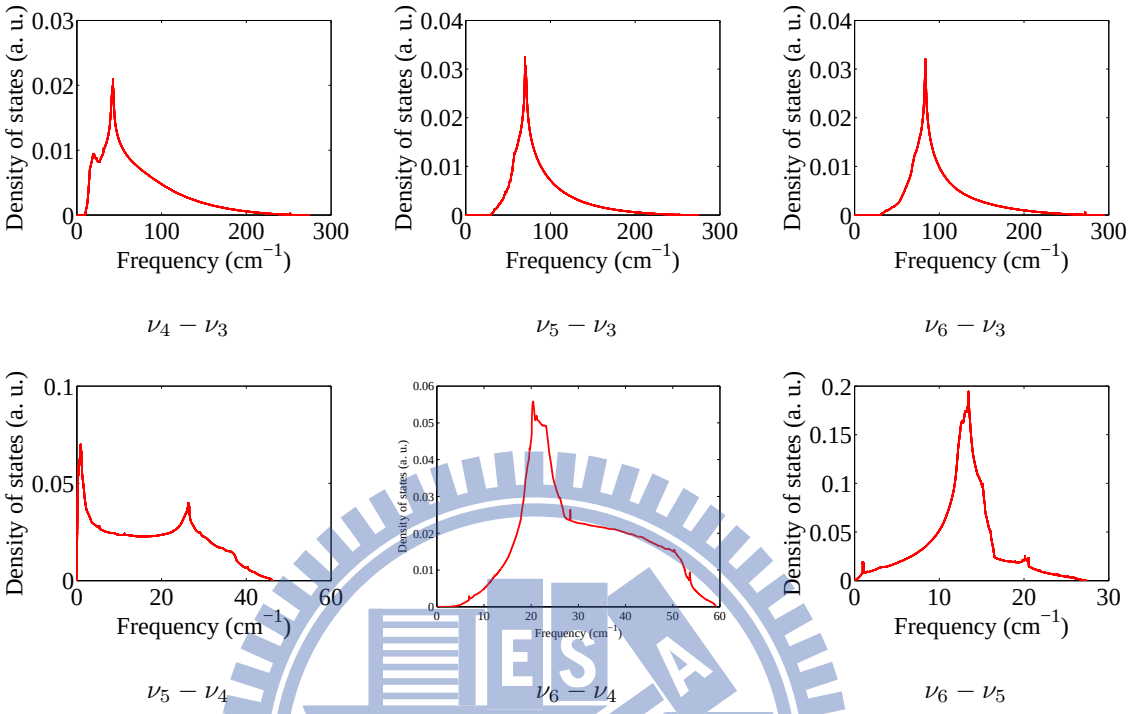


**Figure A.4:** Individual two phonon density of states for GaAs with branched combinations $\nu_4 - \nu_3$, $\nu_5 - \nu_3$, $\nu_6 - \nu_3$, $\nu_5 - \nu_4$, $\nu_6 - \nu_4$, $\nu_6 - \nu_5$.

# A.2 Individual two phonon density of states for InP

## A.2.1 Sum process

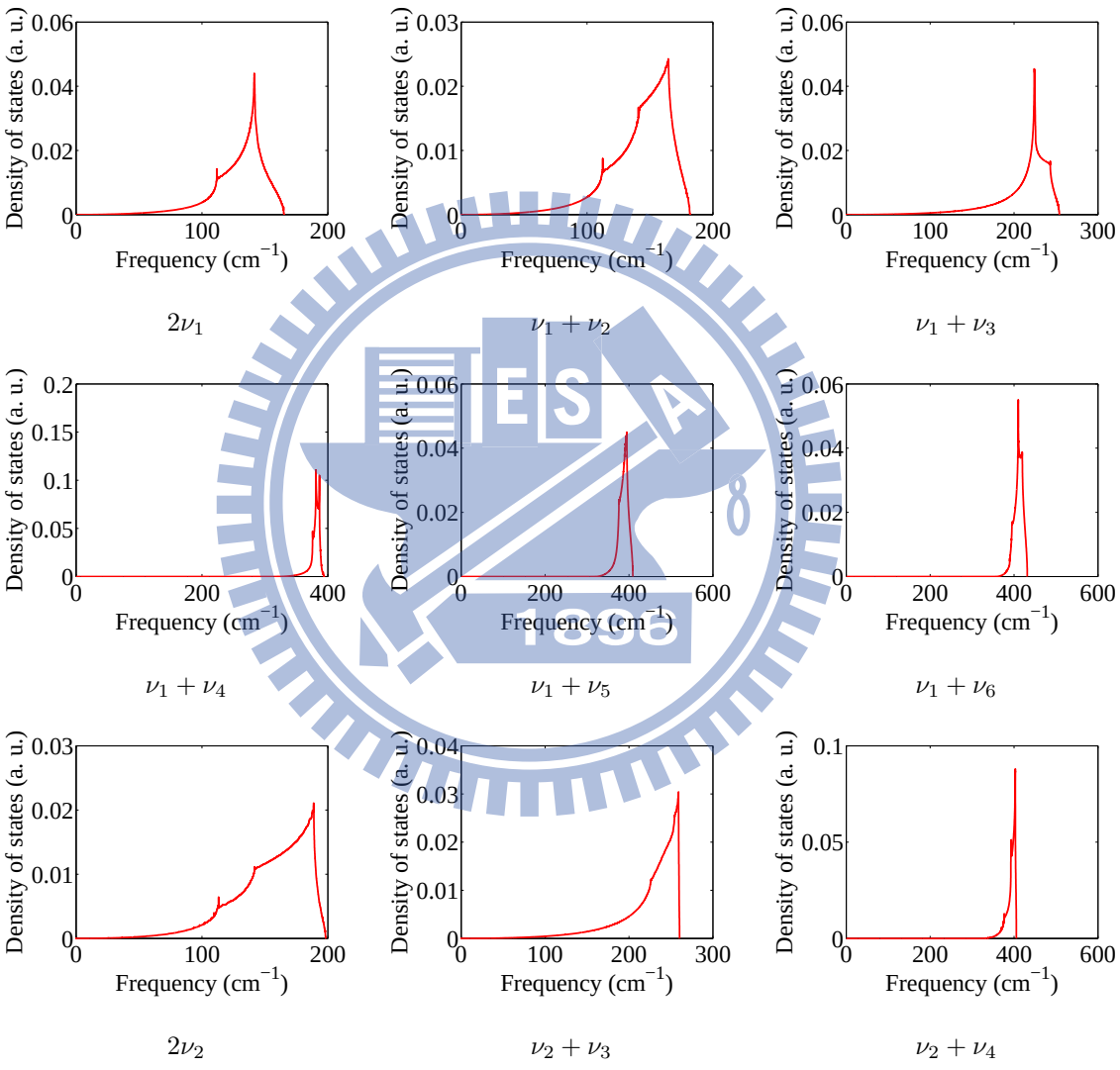


**Figure A.5:** Individual two phonon density of states for InP with branches combinations $2\nu_1$, $\nu_1 + \nu_2$, $\nu_1 + \nu_3$, $\nu_1 + \nu_4$, $\nu_1 + \nu_5$, $\nu_1 + \nu_6$, $2\nu_2$, $\nu_2 + \nu_3$, $\nu_2 + \nu_4$.

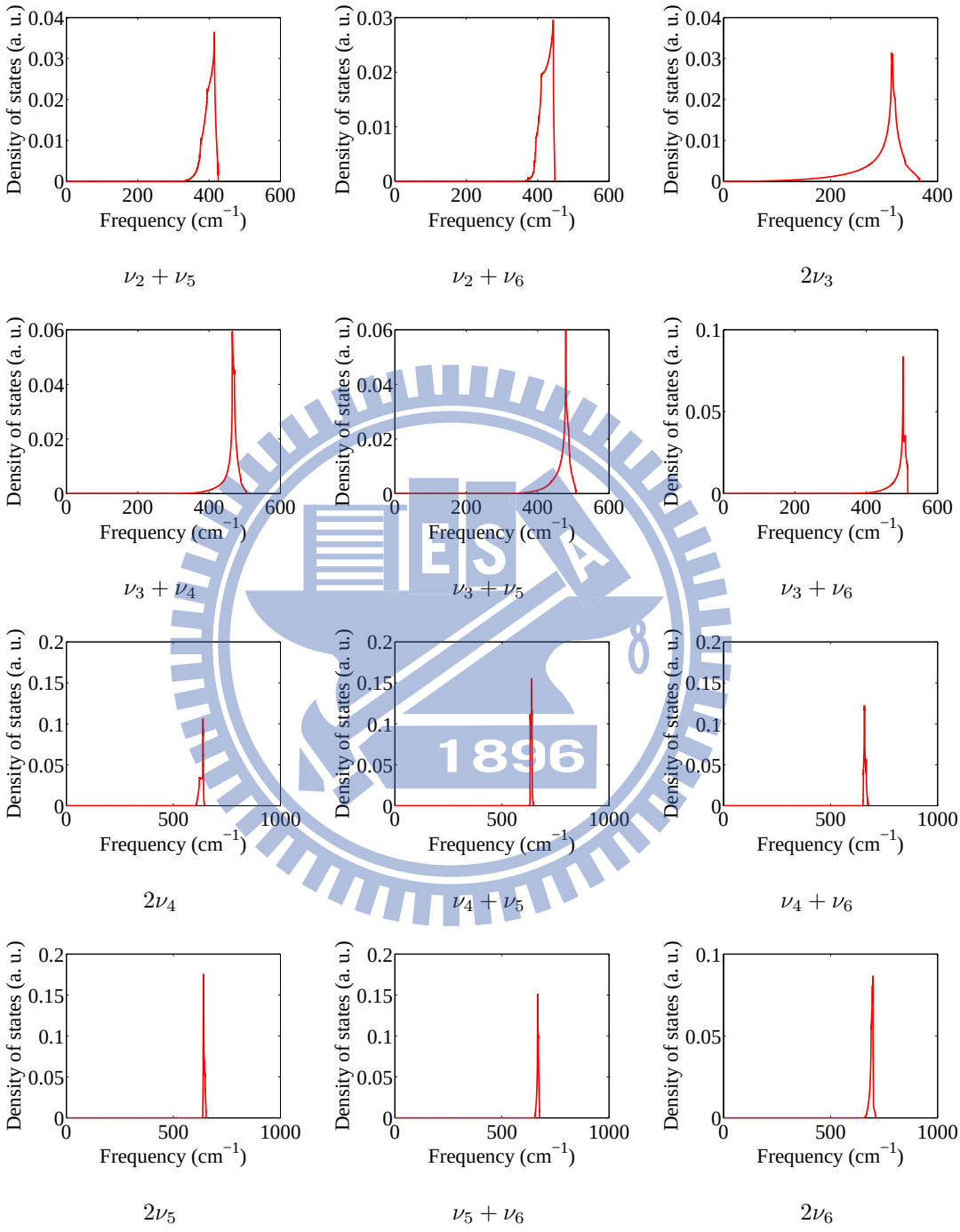


**Figure A.6:** Individual two phonon density of states for InP with branched combinations $\nu_2+\nu_5$, $\nu_2+\nu_6$, $2\nu_3$, $\nu_3+\nu_4$, $\nu_3+\nu_5$, $\nu_3+\nu_6$, $2\nu_4$, $\nu_4+\nu_5$, $\nu_4+\nu_6$, $2\nu_5$, $\nu_5+\nu_6$, $2\nu_6$.

### A.2.2 Difference process

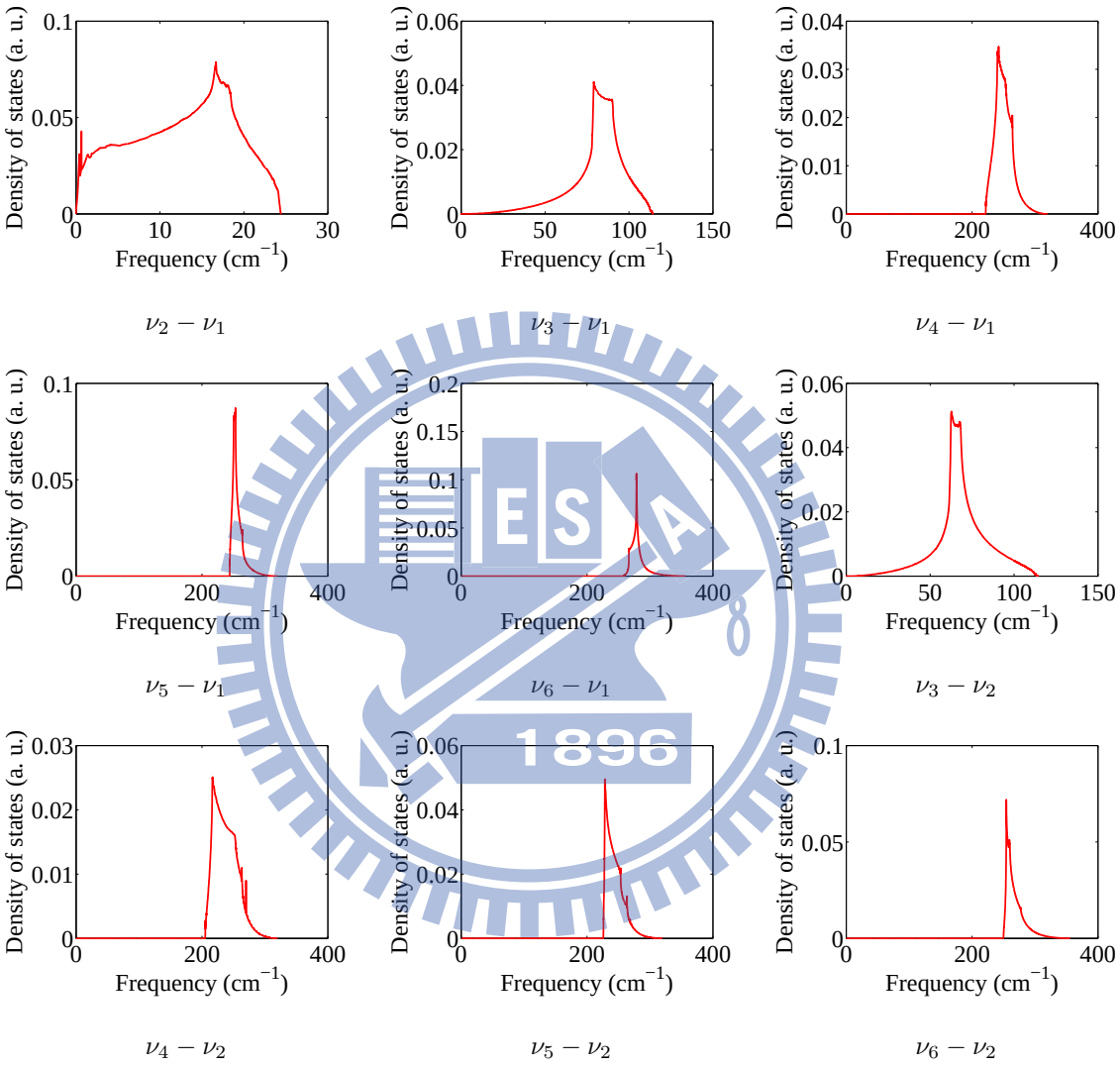


**Figure A.7:** Individual two phonon density of states for InP with branched combinations $\nu_2 - \nu_1$, $\nu_3 - \nu_1$, $\nu_4 - \nu_1$, $\nu_5 - \nu_1$, $\nu_6 - \nu_1$, $\nu_3 - \nu_2$, $\nu_4 - \nu_2$, $\nu_5 - \nu_2$, $\nu_6 - \nu_2$.

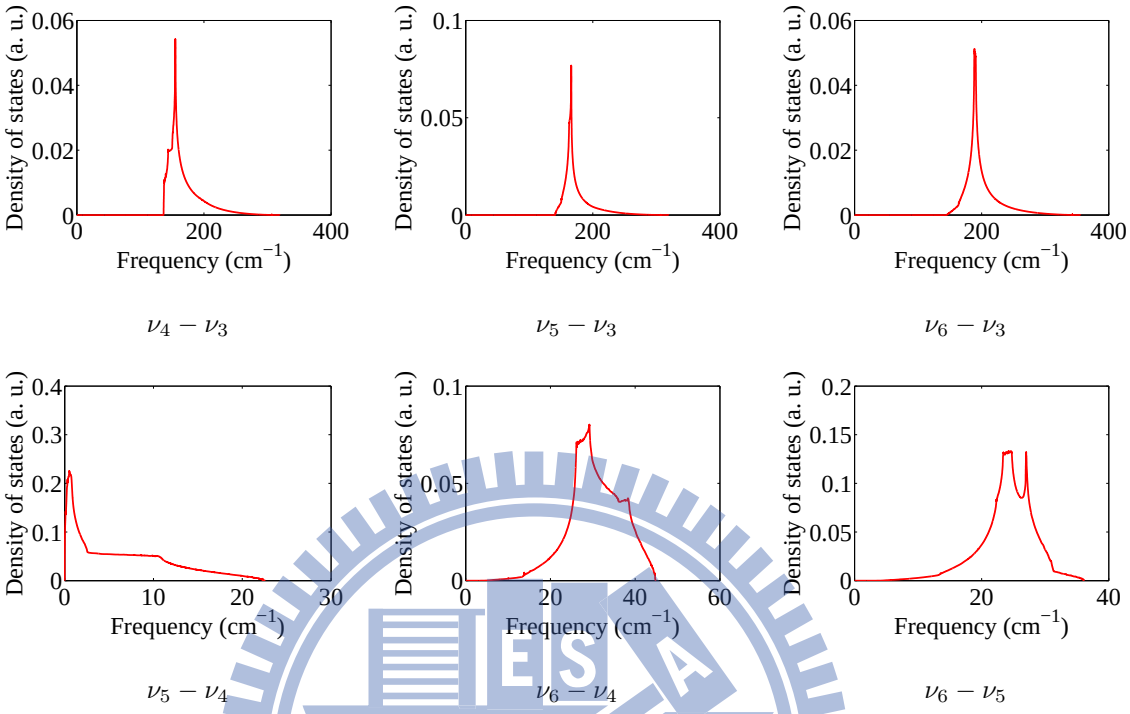


**Figure A.8:** Individual two phonon density of states for InP with branched combinations $\nu_4 - \nu_3$, $\nu_5 - \nu_3$, $\nu_6 - \nu_3$, $\nu_5 - \nu_4$, $\nu_6 - \nu_4$, $\nu_6 - \nu_5$.

## A.3 Spectral feature assignment for GaAs

| Feature type | Position ($cm^{-1}$) | Branch combination | Critical points |
|---|---|---|---|
| $P_0$ | 9.8 | $\nu_4 - \nu_3$ | W(0.5,1,0) |
| P | 12.4 | $\nu_2 - \nu_1$ | W(0.5,1,0) |
| P | 13.5 | $\nu_6 - \nu_5$ | L(0.5,0.5,0.5) |
| $P_2$ | 15.2 | $\nu_6 - \nu_5$ | W(0.5,1,0) |
| P | 19.41 | $\nu_2 - \nu_1$ | Q(0.5,0.77,0.23) |
| P | 20.12 | $\nu_6 - \nu_5$ | $\Sigma$(0.59,0.59,0) |
| P | 20.4 | $\nu_6 - \nu_4$ | $\Lambda$(0.05,0.05,0.05) |
| $P_2$ | 23.2 | $\nu_6 - \nu_4$ | $\Gamma$XWK(0.22,0.48,0) |
| P | 26.3 | $\nu_5 - \nu_4$ | L(0.5,0.5,0.5) |
| $P_3$ | 27 | $\nu_6 - \nu_4$ | L(0.5,0.5,0.5) |
| $P_0$ | 27.1 | $\nu_4 - \nu_3$ | L(0.5,0.5,0.5) |
| $P_3$ | 27.4 | $\nu_6 - \nu_5$ | $\Delta$(0,0.43,0) |
| $P_0$ | 30 | $\nu_{5,6} - \nu_3$ | X(0,1,0) |
| $P_3$ | 35.7 | $\nu_2 - \nu_1$ | $\Sigma$(0.67,0.67,0) |
| $P_2$ | 37.9 | $\nu_5 - \nu_4$ | $\Sigma$(0.71,0.71,0) |
| P | 42.7 | $\nu_4 - \nu_3$ | Q(0.5,0.73,0.27) |
| $P_3$ | 46.2 | $\nu_5 - \nu_4$ | W(0.5,1,0) |
| $P_0$ | 51.5 | $\nu_{5,6} - \nu_3$ | L(0.5,0.5,0.5) |
| $P_2$ | 53.6 | $\nu_6 - \nu_4$ | $\Sigma$(0.69,0.69,0) |
| $P_1$ | 57.2 | $\nu_5 - \nu_3$ | W(0.5,1,0) |
| $P_3$ | 59.2 | $\nu_6 - \nu_4$ | W(0.5,1,0) |

*continued on next page*

*continued from previous page*

| Feature type | Position ($cm^{-1}$) | Branch combination | Critical points |
|---|---|---|---|
| $P_1$ | 68.2 | $\nu_6 - \nu_3$ | W(0.5,1,0) |
| P | 69.9 | $\nu_5 - \nu_3$ | Q(0.5,0.76,0.24) |
| P | 74.5 | $\nu_3 - \nu_2$ | Q(0.5,0.84,0.16) |
| $P_2$ | 81.4 | $\nu_3 - \nu_2$ | W(0.5,1,0) |
| P | 83.6 | $\nu_6 - \nu_3$ | Q(0.5,0.78,0.22) |
| $P_0$ | 92.1 | $\nu_4 - \nu_2$ | W(0.5,1,0) |
| P | 93.8 | $\nu_3 - \nu_1$ | W(0.5,1,0) |
| $P_0$ | 98.1 | $\nu_4 - \nu_2$ | $\Sigma$(0.7,0.7,0) |
| $P_0$ | 104.5 | $\nu_4 - \nu_1$ | W(0.5,1,0) |
| $P_2$ | 106.1 | $\nu_3 - \nu_1$ | $\Gamma$KL(0.66,0.66,0.18) |
| $P_1$ | 128.1 | $2\nu_1$ | L(0.5,0.5,0.5) |
| $P_1$ | 130.2 | $\nu_1 + \nu_2$ | L(0.5,0.5,0.5) |
| $P_1$ | 132.8 | $2\nu_2$ | L(0.5,0.5,0.5) |
| $P_1$ | 133 | $\nu_4 - \nu_1$ | $\Sigma$(0.72,0.72,0) |
| $P_0$ | 136 | $\nu_5 - \nu_2$ | $\Sigma$(0.68,0.68,0) |
| P | 138.2 | $\nu_5 - \nu_2$ | W(0.5,1,0) |
| $P_3$ | 148.5 | $\nu_3 - \nu_{1,2}$ | L(0.5,0.5,0.5) |
| $P_0$ | 150.8 | $\nu_5 - \nu_1$ | W(0.5,1,0) |
| $P_0$ | 151 | $\nu_6 - \nu_2$ | W(0.5,1,0) |
| P | 151.8 | $\nu_6 - \nu_2$ | $\Sigma$(0.72,0.72,0) |
| P | 161.5 | $\nu_4 - \nu_{1,2}$ | X(0,1,0) |
| $P_0$ | 163.8 | $\nu_6 - \nu_1$ | W(0.5,1,0) |
| P | 165.4 | $2\nu_1$ | S(0.14,1,0.14) |
| $P_1$ | 165.9 | $\nu_{1,2} + \nu_2$ | X(0,1,0) |

*continued on next page*

*continued from previous page*

| Feature type | Position ($cm^{-1}$) | Branch combination | Critical points |
|---|---|---|---|
| $P_2$ | 171 | $\nu_{5,6} - \nu_2$ | X(0,1,0) |
| P | 171.6 | $\nu_5 - \nu_1$ | S(0.16,1,0.16) |
| $P_2$ | 171.6 | $\nu_4 - \nu_2$ | $\Delta$(0,0.8,0) |
| P | 172.6 | $\nu_4 - \nu_1$ | L(0.5,0.5,0.5) |
| $P_3$ | 172.6 | $\nu_4 - \nu_2$ | L(0.5,0.5,0.5) |
| $P_2$ | 198 | $\nu_{5,6} - \nu_2$ | L(0.5,0.5,0.5) |
| P | 201.1 | $\nu_6 - \nu_1$ | L(0.5,0.5,0.5) |
| $P_2$ | 201.1 | $\nu_5 - \nu_1$ | L(0.5,0.5,0.5) |
| P | 201.1 | $\nu_1 + \nu_2$ | $\Sigma$(0.67,0.67,0) |
| $P_3$ | 207.1 | $2\nu_1$ | W(0.5,1,0) |
| $P_3$ | 219.5 | $\nu_1 + \nu_2$ | W(0.5,1,0) |
| P | 232 | $2\nu_2$ | W(0.5,1,0) |
| $P_3$ | 237.2 | $2\nu_2$ | $\Sigma$(0.67,0.67,0) |
| P | 265.8 | $\nu_1 + \nu_3$ | $\Gamma$KL(0.62,0.62,0.25) |
| $P_3$ | 278 | $\nu_1 + \nu_3$ | L(0.5,0.5,0.5) |
| $P_1$ | 278 | $\nu_2 + \nu_3$ | L(0.5,0.5,0.5) |
| $P_0$ | 299 | $\nu_1 + \nu_4$ | L(0.5,0.5,0.5) |
| $P_2$ | 301.2 | $\nu_1 + \nu_3$ | W(0.5,1,0) |
| $P_1$ | 302.4 | $\nu_1 + \nu_4$ | L(0.5,0.5,0.5) |
| $P_0$ | 302.4 | $\nu_2 + \nu_4$ | L(0.5,0.5,0.5) |
| $P_3$ | 306.6 | $\nu_1 + \nu_3$ | X(0,1,0) |
| P | 306.6 | $\nu_2 + \nu_3$ | X(0,1,0) |
| $P_1$ | 307.5 | $\nu_1 + \nu_4$ | $\Gamma$KL(0.61,0.61,0.21) |
| $P_2$ | 312.9 | $\nu_2 + \nu_3$ | W(0.5,1,0) |

*continued on next page*

*continued from previous page*

| Feature type | Position ($cm^{-1}$) | Branch combination | Critical points |
|---|---|---|---|
| P | 313.2 | $\nu_1 + \nu_4$ | W(0.5,1,0) |
| P | 319.1 | $\nu_1 + \nu_4$ | Σ(0.38,0.38,0) |
| $P_3$ | 319.5 | $\nu_2 + \nu_3$ | K(0.75,0.75,0) |
| $P_2$ | 322.8 | $\nu_1 + \nu_4$ | ΓXUL(0.26,0.36,0.26) |
| $P_0$ | 326.6 | $\nu_2 + \nu_4$ | ΓXUL(0.31,0.35,0.31) |
| $P_1$ | 330.5 | $\nu_1 + \nu_{5,6}$, $\nu_2 + \nu_6$ | L(0.5,0.5,0.5) |
| $P_1$ | 335.5 | $\nu_1 + \nu_6$ | Λ(0.24,0.24,0.24) |
| $P_3$ | 335.9 | $\nu_1 + \nu_4$ | Δ(0,0.83,0) |
| $P_1$ | 335.9 | $\nu_2 + \nu_4$ | Δ(0,0.83,0) |
| $P_1$ | 337 | $\nu_2 + \nu_6$ | Λ(0.23,0.23,0.23) |
| P | 337.1 | $\nu_1 + \nu_5$ | X(0,1,0) |
| $P_1$ | 337.6 | $\nu_2 + \nu_5$ | Δ(0,0.82,0) |
| P | 338.4 | $\nu_2 + \nu_4$ | ΓKL(0.66,0.66,0.13) |
| $P_2$ | 342.4 | $\nu_2 + \nu_4$ | ΓXWK(0.33,0.64,0) |
| $P_3$ | 346.4 | $\nu_2 + \nu_4$ | ΓXUL(0.2,0.69,0.2) |
| $P_1$ | 349.2 | $\nu_1 + \nu_6$ | ΓXUL(0.19,0.7,0.19) |
| P | 352 | $\nu_1 + \nu_6$ | Σ(0.57,0.57,0) |
| P | 354 | $\nu_1 + \nu_6$ | Δ(0,0.52,0) |
| $P_3$ | 357.7 | $\nu_1 + \nu_5$ | W(0.5,1,0) |
| P | 358.8 | $\nu_2 + \nu_6$ | Δ(0,0.52,0) |
| P | 370.4 | $\nu_2 + \nu_5$ | W(0.5,1,0) |
| $P_3$ | 370.7 | $\nu_1 + \nu_6$ | W(0.5,1,0) |
| P | 372.2 | $\nu_3 + \nu_3$ | Q(0.5,0.78,0.22) |
| $P_3$ | 373.4 | $\nu_2 + \nu_5$ | Σ(0.66,0.66,0) |

*continued on next page*

*continued from previous page*

| Feature type | Position ($cm^{-1}$) | Branch combination | Critical points |
|---|---|---|---|
| P | 384 | $\nu_2 + \nu_6$ | W(0.5,1,0) |
| $P_3$ | 389.7 | $\nu_2 + \nu_6$ | Σ(0.64,0.64,0) |
| $P_2$ | 397.5 | $3\nu_3$ | W(0.5,1,0) |
| P | 406.8 | $\nu_3 + \nu_4$ | W(0.5,1,0) |
| $P_2$ | 415.6 | $\nu_3 + \nu_4$ | ΓXUL(0.27,0.72,0.72) |
| $P_0$ | 416.1 | $2\nu_4$ | W(0.5,1,0) |
| $P_3$ | 428 | $2\nu_3$ | L(0.5,0.5,0.5) |
| $P_1$ | 433 | $2\nu_4$ | Σ(0.71,0.71,0) |
| P | 442.5 | $\nu_3 + \nu_5$ | Q(0.5,0.8,0.2) |
| $P_3$ | 449 | $\nu_3 + \nu_4$ | L(0.5,0.5,0.5) |
| $P_2$ | 451.6 | $\nu_3 + \nu_5$ | W(0.5,1,0) |
| P | 455.6 | $\nu_3 + \nu_6$ | Q(0.5,0.78,0.22) |
| $P_2$ | 457.6 | $\nu_3 + \nu_6$ | ΓKL(0.64,0.64,0.19) |
| $P_0$ | 462 | $\nu_4 + \nu_5$ | W(0.5,1,0) |
| $P_2$ | 465.5 | $\nu_3 + \nu_6$ | W(0.5,1,0) |
| $P_3$ | 467.8 | $\nu_3 + \nu_4$ | X(0,1,0) |
| $P_0$ | 470 | $\nu_4 + \nu_5$ | Σ(0.72,0.72,0) |
| $P_0$ | 475.3 | $\nu_4 + \nu_6$ | W(0.5,1,0) |
| P | 475.9 | $2\nu_4$ | L(0.5,0.5,0.5) |
| $P_3$ | 477.8 | $\nu_3 + \nu_{5,6}$ | L(0.5,0.5,0.5) |
| $P_1$ | 484 | $\nu_4 + \nu_6$ | Σ(0.73,0.73,0) |
| P | 496.1 | $\nu_4 + \nu_5$ | X(0,1,0) |
| $P_1$ | 496.8 | $\nu_4 + \nu_6$ | X(0,1,0) |
| P | 501.5 | $\nu_4 + \nu_{5,6}$ | L(0.5,0.5,0.5) |

*continued on next page*

*continued from previous page*

| Feature type | Position ($cm^{-1}$) | Branch combination | Critical points |
|---|---|---|---|
| $P_0$ | 507.1 | $2\nu_5$ | S(0.09,1,0.09) |
| $P_0$ | 507.5 | $\nu_{5,6} + \nu_6$ | X(0,1,0) |
| P | 508.5 | $\nu_{4,5} + \nu_5$ | $\Delta$(0,0.8,0) |
| P | 509.2 | $2\nu_4$ | $\Delta$(0,0.73,0) |
| $P_1$ | 521.5 | $\nu_5 + \nu_6$ | W(0.5,1,0) |
| P | 530 | $\nu_5 + \nu_6$ | L(0.5,0.5,0.5) |
| $P_2$ | 530 | $2\nu_5$ | L(0.5,0.5,0.5) |
| $P_0$ | 530 | $2\nu_6$ | L(0.5,0.5,0.5) |
| $P_2$ | 532 | $\nu_4 + \nu_{4,5}$ | $\Lambda$(0.31,0.31,0.31) |
| $P_1$ | 534.5 | $2\nu_6$ | W(0.5,1,0) |
| P | 538.8 | $\nu_6 + \nu_6$ | Q(0.5,0.75,0.25) |
| $P_3$ | 549.9 | $\nu_{4,5} + \nu_{4,5}$ | $\Gamma$(0,0,0) |
| $P_3$ | 570 | $\nu_{4,5} + \nu_6$ | $\Gamma$(0,0,0) |
| $P_3$ | 590.1 | $\nu_6 + \nu_6$ | $\Gamma$(0,0,0) |

**Table A.1:** Two phonon spectral feature assignment for GaAs

## A.4 Spectral feature assignment for InP

| Feature type | Position ($cm^{-1}$) | Branch combination | Critical points |
|---|---|---|---|
| P | 0.52 | $\nu_5 - \nu_4$ | Q(0.5,0.54,0.46) |
| $P_3$ | 2.79 | $\nu_5 - \nu_4$ | Σ(0.32,0.32,0) |
| $P_2$ | 10.4 | $\nu_5 - \nu_4$ | U(0.25,1,0.25) |
| $P_0$ | 13 | $\nu_6 - \nu_{4,5}$ | L(0.5,0.5,0.5) |
| P | 16.66 | $\nu_2 - \nu_1$ | W(0.5,1,0) |
| $P_1$ | 18.08 | $\nu_2 - \nu_1$ | Q(0.5,0.78,0.22) |
| $P_1$ | 22.3 | $\nu_6 - \nu_5$ | W(0.5,1,0) |
| $P_3$ | 22.6 | $\nu_5 - \nu_4$ | W(0.5,1,0) |
| $P_1$ | 24.23 | $\nu_6 - \nu_5$ | Q(0.5,0.79,0.21) |
| $P_3$ | 24.43 | $\nu_2 - \nu_1$ | Σ(0.65,0.65,0) |
| $P_1$ | 26.2 | $\nu_6 - \nu_4$ | ΓXUL(0.18,0.52,0.18) |
| P | 27.01 | $\nu_6 - \nu_5$ | Σ(0.33,0.33,0) |
| P | 29.2 | $\nu_6 - \nu_5$ | Σ(0.33,0.33,0) |
| $P_3$ | 31.3 | $\nu_6 - \nu_5$ | Σ(0.53,0.53,0) |
| $P_3$ | 36.1 | $\nu_6 - \nu_{4,5}$ | Γ(0,0,0) |
| P | 38.3 | $\nu_6 - \nu_4$ | Σ(0.65,0.65,0) |
| $P_3$ | 44.9 | $\nu_6 - \nu_4$ | W(0.5,1,0) |
| P | 62.7 | $\nu_3 - \nu_2$ | W(0.5,1,0) |
| P | 67.41 | $\nu_3 - \nu_2$ | ΓXUL(0.27,0.73,0.27) |
| P | 79.09 | $\nu_3 - \nu_1$ | W(0.5,1,0) |
| $P_1$ | 89.92 | $\nu_3 - \nu_1$ | ΓXUL(0.31,0.78,0.31) |

*continued on next page*

*continued from previous page*

| Feature type | Position ($cm^{-1}$) | Branch combination | Critical points |
|---|---|---|---|
| $P_1$ | 111.9 | $\nu_{1,2} + \nu_{1,2}$ | L(0.5,0.5,0.5) |
| $P_3$ | 112.8 | $\nu_3 - \nu_1$ | X(0,1,0) |
| $P_3$ | 114.5 | $\nu_3 - \nu_2$ | L(0.5,0.5,0.5) |
| $P_0$ | 136.3 | $\nu_4 - \nu_3$ | Z(0.17,1,0) |
| $P_1$ | 137.1 | $\nu_4 - \nu_3$ | S(0.11,1,0.11) |
| $P_0$ | 140.7 | $\nu_5 - \nu_3$ | X(0,1,0) |
| P | 142 | $2\nu_1$ | X(0,1,0) |
| $P_1$ | 142 | $\nu_1 + \nu_2$ | X(0,1,0) |
| $P_1$ | 142 | $2\nu_2$ | X(0,1,0) |
| $P_1$ | 143.6 | $\nu_4 - \nu_3$ | W(0.5,1,0) |
| $P_0$ | 150 | $\nu_{4,5} - \nu_3$ | L(0.5,0.5,0.5) |
| P | 155 | $\nu_4 - \nu_3$ | Q(0.5,0.72,0.28) |
| $P_1$ | 162.6 | $\nu_5 - \nu_3$ | ΓXUL(0.35,0.79,0.35) |
| $P_0$ | 163 | $\nu_6 - \nu_3$ | L(0.5,0.5,0.5) |
| P | 164.6 | $\nu_1 + \nu_2$ | Σ(0.7,0.7,0) |
| $P_3$ | 165.4 | $2\nu_1$ | W(0.5,1,0) |
| P | 166.1 | $\nu_5 - \nu_3$ | W(0.5,1,0) |
| $P_3$ | 182 | $\nu_1 + \nu_2$ | W(0.5,1,0) |
| P | 188.6 | $\nu_6 - \nu_3$ | W(0.5,1,0) |
| P | 188.7 | $2\nu_2$ | Σ(0.67,0.67,0) |
| $P_3$ | 198.6 | $2\nu_2$ | W(0.5,1,0) |
| $P_0$ | 204.8 | $\nu_4 - \nu_2$ | W(0.5,1,0) |
| P | 216.8 | $\nu_4 - \nu_2$ | Σ(0.69,0.69,0) |
| $P_0$ | 221.4 | $\nu_4 - \nu_1$ | W(0.5,1,0) |

*continued on next page*

*continued from previous page*

| Feature type | Position ($cm^{-1}$) | Branch combination | Critical points |
|---|---|---|---|
| P | 224.1 | $\nu_1 + \nu_3$ | L(0.5,0.5,0.5) |
| $P_0$ | 225.9 | $\nu_5 - \nu_2$ | Σ(0.65,0.65,0) |
| $P_1$ | 226.2 | $\nu_2 + \nu_3$ | L(0.5,0.5,0.5) |
| P | 228.7 | $\nu_5 - \nu_2$ | W(0.5,1,0) |
| P | 240.5 | $\nu_4 - \nu_1$ | Σ(0.73,0.73,0) |
| $P_0$ | 244 | $\nu_5 - \nu_1$ | W(0.5,1,0) |
| P | 250.4 | $\nu_5 - \nu_1$ | Σ(0.65,0.65,0) |
| $P_2$ | 252.3 | $\nu_4 - \nu_{1,2}$ | Δ(0,0.77,0) |
| P | 253.3 | $\nu_5 - \nu_1$ | X(0,1,0) |
| $P_2$ | 253.3 | $\nu_5 - \nu_2$ | X(0,1,0) |
| $P_3$ | 254.2 | $\nu_1 + \nu_3$ | X(0,1,0) |
| $P_1$ | 254.2 | $\nu_2 + \nu_3$ | X(0,1,0) |
| P | 254.4 | $\nu_6 - \nu_2$ | Σ(0.72,0.72,0) |
| $P_0$ | 257.1 | $\nu_6 - \nu_1$ | X(0,1,0) |
| P | 259 | $\nu_2 - \nu_3$ | W(0.5,1,0) |
| $P_2$ | 259.2 | $\nu_6 - \nu_2$ | W(0.5,1,0) |
| $P_2$ | 263.9 | $\nu_{4,5} - \nu_{1,2}$ | L(0.5,0.5,0.5) |
| $P_1$ | 266.5 | $\nu_6 - \nu_1$ | W(0.5,1,0) |
| P | 278.6 | $\nu_6 - \nu_{1,2}$ | W(0.5,1,0) |
| P | 314.3 | $2\nu_3$ | Q(0.5,0.78,0.22) |
| $P_2$ | 321 | $2\nu_3$ | W(0.5,1,0) |
| $P_2$ | 340 | $2\nu_3$ | L(0.5,0.5,0.5) |
| $P_3$ | 366.9 | $2\nu_3$ | X(0,1,0) |
| $P_1$ | 375.8 | $\nu_{1,2} + \nu_{4,5}$ | L(0.5,0.5,0.5) |

*continued on next page*

*continued from previous page*

| Feature type | Position ($cm^{-1}$) | Branch combination | Critical points |
|---|---|---|---|
| P | 381.2 | $\nu_1 + \nu_4$ | Σ(0.65,0.65,0) |
| P | 386.7 | $\nu_1 + \nu_4$ | W(0.5,1,0) |
| $P_0$ | 388.8 | $\nu_{1,2} + \nu_6$ | L(0.5,0.5,0.5) |
| P | 393.3 | $\nu_2 + \nu_4$ | S(0.06,1,0.06) |
| $P_3$ | 394.6 | $\nu_1 + \nu_4$ | X(0,1,0) |
| P | 394.6 | $\nu_1 + \nu_5$ | X(0,1,0) |
| $P_1$ | 394.9 | $\nu_1 + \nu_6$ | Λ(0.3,0.3,03) |
| $P_1$ | 395 | $\nu_2 + \nu_5$ | X(0,1,0) |
| $P_1$ | 398.4 | $\nu_2 + \nu_6$ | X(0,1,0) |
| P | 402.9 | $\nu_2 + \nu_4$ | W(0.5,1,0) |
| $P_3$ | 409.4 | $\nu_1 + \nu_5$ | W(0.5,1,0) |
| P | 410.4 | $\nu_1 + \nu_6$ | Δ(0,0.56,0) |
| $P_1$ | 410.4 | $\nu_2 + \nu_6$ | Δ(0,0.56,0) |
| P | 414.7 | $\nu_2 + \nu_5$ | Σ(0.7,0.7,0) |
| P | 419.5 | $\nu_1 + \nu_6$ | Σ(0.66,0.66,0) |
| $P_3$ | 426 | $\nu_1 + \nu_6$ | W(0.5,1,0) |
| $P_3$ | 431.6 | $\nu_1 + \nu_6$ | W(0.5,1,0) |
| P | 443.7 | $\nu_2 + \nu_6$ | Σ(0.65,0.65,0) |
| $P_3$ | 448.3 | $\nu_2 + \nu_6$ | W(0.5,1,0) |
| P | 465.3 | $\nu_3 + \nu_4$ | W(0.5,1,0) |
| $P_2$ | 470.9 | $\nu_3 + \nu_4$ | ΓXUL(0.32,0.78,0.32) |
| P | 479 | $\nu_3 + \nu_5$ | Q(0.5,0.75,0.25) |
| $P_2$ | 487 | $\nu_3 + \nu_5$ | W(0.5,1,0) |
| $P_3$ | 490.3 | $\nu_3 + \nu_4$ | L(0.5,0.5,0.5) |

*continued on next page*

*continued from previous page*

| Feature type | Position ($cm^{-1}$) | Branch combination | Critical points |
|---|---|---|---|
| P | 503.1 | $\nu_3 + \nu_6$ | L(0.5,0.5,0.5) |
| $P_3$ | 507.7 | $\nu_3 + \nu_{4,5}$ | X(0,1,0) |
| P | 509.4 | $\nu_3 + \nu_6$ | W(0.5,1,0) |
| $P_3$ | 516.7 | $\nu_3 + \nu_6$ | S(0.14,1,0.14) |
| $P_0$ | 608.2 | $2\nu_4$ | W(0.5,1,0) |
| P | 623.3 | $2\nu_4$ | Σ(0.71,0.71,0) |
| P | 631.6 | $\nu_4 + \nu_5$ | W(0.5,1,0) |
| P | 638.3 | $\nu_4 + \nu_{4,5}$ | Γ(0,0,0) |
| $P_0$ | 639.3 | $2\nu_5$ | Γ(0,0,0) |
| $P_3$ | 640.3 | $\nu_4 + \nu_5$ | L(0.5,0.5,0.5) |
| P | 640.3 | $2\nu_5$ | L(0.5,0.5,0.5) |
| $P_3$ | 647.3 | $2\nu_4$ | Δ(0,0.84,0) |
| $P_2$ | 648.3 | $2\nu_5$ | X(0,1,0) |
| $P_0$ | 653 | $\nu_4 + \nu_6$ | W(0.5,1,0) |
| $P_0$ | 653.3 | $\nu_{4,5} + \nu_6$ | L(0.5,0.5,0.5) |
| $P_3$ | 653.4 | $2\nu_5$ | W(0.5,1,0) |
| P | 658.1 | $\nu_4 + \nu_6$ | Q(0.5,0.75,0.25) |
| $P_1$ | 666.1 | $\nu_5 + \nu_6$ | ΓXUL(0.18,0.62,0.18) |
| $P_0$ | 666.4 | $2\nu_6$ | L(0.5,0.5,0.5) |
| P | 666.5 | $\nu_4 + \nu_6$ | Σ(0.35,0.35,0) |
| P | 667.4 | $\nu_5 + \nu_6$ | ΓXWK(0.52,0.22,0) |
| $P_2$ | 670 | $\nu_5 + \nu_6$ | Σ(0.65,0.65,0) |
| $P_3$ | 675 | $\nu_{4,5} + \nu_6$ | Γ(0,0,0) |
| $P_1$ | 689.5 | $2\nu_6$ | ΓXUL(0.21,0.64,0.21) |

*continued on next page*

| *continued from previous page* | | | |
|---|---|---|---|
| **Feature type** | **Position ($cm^{-1}$)** | **Branch combination** | **Critical points** |
| P | 695.7 | $2\nu_6$ | $\Sigma$(0.34,0.34,0) |
| P | 697.9 | $2\nu_6$ | W(0.5,1,0) |
| $P_3$ | 711.6 | $2\nu_6$ | $\Gamma$(0,0,0) |

**Table A.2:** Two phonon spectral feature assignment for InP

# Bibliography


[1] http://thznetwork.net/index.php/thz-images.

[2] P H Borcherds, G F Alfrey, A D B Woods, and D H Saunderson. Phonon dispersion curves in indium phosphide. *J. Phys. C*, 8(13):2022–2030, 1975.

[3] D Strauch and B Dorner. Phonon dispersion in GaAs. *J. Phys.: Condens. Matter*, 2(6):1457, 1990.

[4] E. S. Koteles and W. R. Datars. Two-phonon absorption in InSb, InAs, and GaAs. *Can. J. Phys.*, 54(16):1676–1682, 1976.

[5] E Bedel, G Landa, R Carles, J P Redoules, and J B Renucci. Raman investigation of the InP lattice dynamics. *J. Phys. C*, 19(10):1471–1479, 1986.

[6] http://en.wikipedia.org/wiki/Terahertz_radiation.

[7] http://www.bbc.com/news/science-environment-18072618.

[8] W. G. Spitzer, editor. *Multiphonon lattice absorption*, volume 3 of *Semiconductors and Semimetals*. Academic Press, New York, 1972.

[9] W. Cochran. Theory of the lattice vibrations of germanium. *Proc. R. Soc. Lond. Ser. A*, 253(1273):260–276, 1959.

[10] K.C. Rustagi and W. Weber. Adiabatic bond charge model for the phonons in $A^3B^5$ semiconductors. *Solid State Commun.*, 18(6):673–675, 1976.

[11] K. Kunc, M. Balkanski, and M. A. Nusimovici. Lattice dynamics of several $A^N B^{8-N}$ compounds having the zincblende structure. ii. numerical calculations. *Phys. Status Solidi (b)*, 72(1):229–248, 1975.

[12] Paolo Giannozzi, Stefano de Gironcoli, Pasquale Pavone, and Stefano Baroni. Ab initio calculation of phonon dispersions in semiconductors. *Phys. Rev. B*, 43:7231–7242, Mar 1991.

[13] G. Deinzer and D. Strauch. Two-phonon infrared absorption spectra of germanium and silicon calculated from first principles. *Phys. Rev. B*, 69:045205, Jan 2004.

[14] Eric L. Shirley and Hadley M. Lawler. Two-phonon infrared spectra of Si and Ge: Calculating and assigning features. *Phys. Rev. B*, 76:054116, Aug 2007.

[15] W. Cochran, S. J. Fray, F. A. Johnson, J. E. Quarrington, and N. Williams. Lattice absorption in gallium arsenide. *J. Appl. Phys.*, 32(10):2102–2106, 1961.

[16] Tomoyuki Sekine, Kunimitsu Uchinokura, and Etsuyuki Matsuura. Two-phonon raman scattering in GaAs. *J. Phys. Chem. Solids*, 38(9):1091–1096, 1977.

[17] B. Ulrici and E. Jahne. Phonon frequencies of InP derived from two-phonon absorption. *Phys. Status Solidi (b)*, 74(2):601–607, 1976.

[18] E.S. Koteles and W.R. Datars. Two-phonon absorption in InP and GaP. *Solid State Commun.*, 19(3):221–225, 1976.

[19] J. P. Perdew and Alex Zunger. Self-interaction correction to density-functional approximations for many-electron systems. *Phys. Rev. B*, 23:5048–5079, May 1981.

[20] D. M. Ceperley and B. J. Alder. Ground state of the electron gas by a stochastic method. *Phys. Rev. Lett.*, 45:566–569, Aug 1980.

[21] Stefano Baroni, Stefano de Gironcoli, Andrea Dal Corso, and Paolo Giannozzi. Phonons and related crystal properties from density-functional perturbation theory. *Rev. Mod. Phys.*, 73:515–562, Jul 2001.

[22] Paolo Giannozzi, Stefano Baroni, Nicola Bonini, Matteo Calandra, Roberto Car, Carlo Cavazzoni, Davide Ceresoli, Guido L Chiarotti, Matteo Cococcioni, Ismaila Dabo, Andrea Dal Corso, Stefano de Gironcoli, Stefano Fabris, Guido Fratesi, Ralph Gebauer, Uwe Gerstmann, Christos Gougoussis, Anton Kokalj, Michele Lazzeri, Layla Martin-Samos, Nicola Marzari, Francesco Mauri, Riccardo Mazzarello, Stefano Paolini, Alfredo Pasquarello, Lorenzo Paulatto, Carlo Sbraccia, Sandro Scandolo, Gabriele Sclauzero, Ari P Seitsonen, Alexander Smogunov, Paolo Umari, and Renata M Wentzcovitch. Quantum espresso: a modular and open-source software project for quantum simulations of materials. *J. Phys.: Condens. Matter*, 21(39):395502, 2009.

[23] Hendrik J. Monkhorst and James D. Pack. Special points for brillouin-zone integrations. *Phys. Rev. B*, 13:5188–5192, Jun 1976.

[24] U. von Barth and R. Car. `www.quantum-espresso.org/pseudopotentials/`.

[25] Peter E. Blöchl, O. Jepsen, and O. K. Andersen. Improved tetrahedron method for brillouin-zone integrations. *Phys. Rev. B*, 49:16223–16233, Jun 1994.

[26] `http://people.sissa.it/~degironc/QE-Tutorial/tutorial_disp.htm`.

[27] J. Fritsch, P. Pavone, and U. Schröder. Ab initio calculation of the phonon dispersion in bulk InP and in the InP(110) surface. *Phys. Rev. B*, 52:11326–11334, Oct 1995.

# 簡歷

姓名：林煌翔 (Huang-Hsiang Lin)

性別：男

籍貫：台灣高雄市

出生：民國 79 年 8 月 15 日

學歷：

國立交通大學　　電機資訊學士班 (2008-2012)

國立交通大學　　電子工程研究所 (2012-2014)

信箱：bob08151990.eecs97@nctu.edu.tw